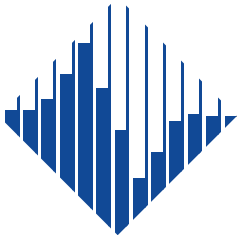

PACIFIC EARTHQUAKE ENGINEERING RESEARCH CENTER

Fire-Induced Structural Collapse on Pier 45 at Fisherman's Wharf, San Francisco, California, May 23, 2020

Mohammadreza Eslami[1,2]
Khalid M. Mosalam[1,3]
Ankit Agrawal[2]
Amarnath Kasalanati[1]

[1]Pacific Earthquake Engineering Research Center
[2]Hinman Consulting Engineers, San Francisco
[3]Department of Civil and Environmental Engineering

PEER Report No. 2021/01

Pacific Earthquake Engineering Research Center
Headquarters at the University of California, Berkeley
January 2021

PEER 2021/01
January 2021

Disclaimer

The opinions, findings, and conclusions or recommendations expressed in this publication are those of the author(s) and do not necessarily reflect the views of the study sponsor(s), the Pacific Earthquake Engineering Research Center, or the Regents of the University of California.

Fire-Induced Structural Collapse on Pier 45 at Fisherman's Wharf, San Francisco, California, May 23, 2020

Mohammadreza Eslami[1,2]

Khalid M. Mosalam[1,3]

Ankit Agrawal[2]

Amarnath Kasalanati[1]

[1]Pacific Earthquake Engineering Research Center

[2]Hinman Consulting Engineers, San Francisco

[3]Department of Civil and Environmental Engineering
University of California, Berkeley

PEER Report No. 2021/01

Pacific Earthquake Engineering Research Center
Headquarters, University of California, Berkeley
January 2021

ABSTRACT

On May 23, 2020, a severe fire resulted in progressive collapse of a processing and storage warehouse structure located at Pier 45, Fisherman's Wharf, in San Francisco, California. This incident provided a unique opportunity to study the performance of structural systems exposed to large open-compartment fires resulting in progressive collapse. Subsequently, a post-fire investigation was conducted to collect data pertinent to both fire severity and key structural characteristics, which were made available to the Pacific Earthquake Engineering Research Center (PEER) at the University of California, Berkeley. The collected information in conjunction with engineering judgment is used to qualitatively and, to the extent possible, quantitatively describe the fire-induced failure modes and damage observed in the structural members. Further, a simplistic sequence of events leading to the fire-induced progressive collapse is hypothesized. Preliminary analysis, based on available fire resistance verification methods, is carried out to qualify this hypothesis. Findings from this report and data available through PEER will contribute towards improving the collective understanding of best practices in performance-based structural fire engineering.

ACKNOWLEDGMENTS

The authors would like to acknowledge the technical and logistical support of the Port of San Francisco, provided by Mr. Rod K. Iwashita, Deputy Director & Chief Harbor Engineer, and Mr. Matthew Bell, Civil Engineer. Moreover, we thank the staff of the Pacific Earthquake Engineering Research Center (PEER) for their effort, particularly the outstanding and timely editing of this report by Ms. Claire Johnson, PEER Technical Editor.

CONTENTS

LIST OF TABLES

LIST OF FIGURES

1 Introduction

1.1 OVERVIEW

In the early hours of May 23, 2020, a fire began in Shed C located at Pier 45 in the historic Fisherman's Wharf neighborhood in San Francisco, California. No loss of life occurred as a result of this severe four-alarm fire,[1] which took 50 engines and 150 fire-fighters nearly seven hours to successfully subdue [Rubenstein and Kroichick [2020]]. Destruction of stored fishing equipment and fire-induced progressive collapse of the warehouse structure resulted in significant direct losses. This incident, in addition to two more recent structure fires, one causing destruction of six commercial buildings in San Francisco [Cabanatuan and Cassidy [2020]] and the other causing partial collapse of a railway bridge in Tempe, Arizona [Tang [2020]], serve as reminders of the significant property loss in that United States that occurs yearly as a consequence of fire [Evarts [2019]].

Given the disastrous consequences of structure fires, performance-based fire engineering design has received significant attention in recent years [Committee [2018]]. Nonetheless, the majority of current design standards and research studies are based on uniform burning assumption, which is not valid for fires in large ($> 100\ m^2$), open-plan compartments, as was the case in the Pier 45 fire [Stern-Gottfried et al. [2010]]. Despite this significant property loss, this incident provides a rare opportunity to study the performance of structural systems under realistic fire exposure in a large open-plan compartment, a common feature of modern architecture. Lessons learnt from fire severity and factors that led to the fire-induced collapse will improve our broader understanding and practices for performance-based structural fire engineering, with special relevance to property owners in the United States. This is viewed as a natural extension of the Performance-Based Earthquake Engineering (PBEE) methodology development by the Pacific Earthquake Engineering Research Center (PEER) for more than two decades.

To this end, a post-fire reconnaissance was conducted by a joint investigation team composed of researchers and practicing engineers from PEER and Hinman Consulting Engineers, San Francisco. Key information pertaining to the timeline of the events, the fire characteristics, and structural details were studied, along with more than 500 photographs as documentary evidence. The documentation and discussion of this information are emphasized in this report. Please note that this Report focuses solely on the effects of fire on the structural system; the cause of the fire is

[1] "Multiple-alarm fire" is a convention used in the United States to quickly communicate the severity and size of a fire. For instance, news outlets report on incidents such as a "four-alarm fire" to indicate a blaze that is more difficult to handle than, say, a "two-alarm fire."

beyond the scope of this Report.

The collected information and accompanying engineering judgment were used to determined, if possible, the sequence of complex interrelated events that led to the fire-induced progressive collapse. In addition, the fire performance metrics of isolated members were compared using simple calculation methods available in published literature and building codes. The findings of this Report will be useful for future and more in-depth analyses and investigations of this fire event. The collected data will be made available through the PEER Center.

1.2 PAST FIRE RECONNAISSANCE EFFORTS

Lessons and experiences derived from past fire reconnaissance efforts have been one of the key themes in fire loss investigation practice and were used to compile this Report. The methodology of post-fire studies in the following incidents were considered herein:

- The final report on the collapse of World Trade Center Towers [of Standards and Technology [2005]];
- The collection of data on fire and collapse of the Faculty of Architecture Building at the Delft University of Technology [Meacham et al. [2009]];
- The fire and collapse of the Faculty of Architecture Building at the Delft University of Technology: Data Collection and Preliminary analyses [Meacham et al. [2010]];
- Investigation of the Windsor Building Fire in Spain [Hironori [2006]];
- Thermal-structural analysis of the MacArthur Maze Freeway collapse [Noble et al. [2008]];
- The collapse of the 16-Story Plasco Building in Tehran due to fire [Ahmadi et al. [2020]];
- The Grenfell Tower fire in Kensington, London [Bisby [2018], Lane [2018], Torero [2018]];
- The fire in the 25-story Aseman Hotel; and
- The Torch Building fire in Dubai [Henderson and Graham [2017]].

1.3 COMMON TECHNIQUES OF FIRE RECONNAISSANCE EFFORTS

In contrast to those reconnaissance efforts due to natural hazards (which typically focus on large regions affected by earthquakes, hurricanes, floods etc., see those investigations conducted by the Structural Extreme Events Reconnaissance (StEER) Network[2]), structural fire reconnaissance focuses on the structural damage and health monitoring of a particular building damaged by the fire or, in the case of large fires, on a limited number of buildings in the vicinity of that building.

[2] https://www.steer.network/.

In general, it is difficult to pinpoint the ignition source of the fire and its path, especially in the case of a fire that escalates to several alarms, hampering the structural fire reconnaissance effort that takes place after the fire is suppressed. This is particularly the case when the affected building is large in terms of its square feet and complex architectural design, or whether it is connected to other buildings. Therefore, rapid response and the gathering of recorded information by the fire fighters and early responders while the fire is occurring are essential for meaningful structural fire reconnaissance efforts.

In order to facilitate simulation and analysis of a fire event, it is important to gather sufficient data and information, which include the following: (a) developing a time history of the incident; (b) determining the ignition source; and (c) establishing those factors contributing to the fire growth, including those strategies that successfully suppressed the spread of fire and those critical failures that contributed to its spread [Meacham et al. [2009]].

Successful fire simulation and meaningful analysis require obtaining pre-fire history and trans-fire information. The following summarizes the types of pre-fire and trans-fire data, and information desired for a best-practice evaluation of an event [Lilley [1997], of Fire Chiefs and of Arson Investigators [2014]].

Pre-Fire Data and Information: Pre-fire data and information describes the condition of the building, training of the occupants, and emergency response procedures in place prior to the fire event, and includes:

1. Immediate access to architectural, structural, mechanical, electrical, plumbing, and fire protection features of building as built and at the time of the fire;

2. Immediate access on the building's occupancy classification, including contents, etc.; and

3. Immediate access to the facility's emergency management procedures and protocols.

Trans-Fire Event Data and Information: Trans-fire events are those events from the point of established burning to extinguishment. Data regarding trans-fire events can be obtained from photographs and video recordings at all stages of the fire, as well as interviews with first responders to determine the "history" of the blaze and actions taken on the scene to mitigate the spread of fire [Meacham et al. [2010], Buchanan and Abu [2017]].

Collection of these types of data and information are consistent with other investigations of significant fire-related structural collapses, including those of World Trade Center towers,the Faculty of Architecture Building at Delft University of Technology, the MacArthur Maze Freeway, and the Plasco Building.

A critical aspect to this specific project was to establish relationships with local personnel who had access to data, information, and personnel of interest. This was accomplished by collaborating with San Francisco Fire Department and the Executive Team of Port of San Francisco. Prior to the site visit to Shed C, an initial walk-through of Shed A was arranged, which was identical in construction to Shed C and provided a unique opportunity to see the building "before fire." The walk-through, site visit, and discussions included the following research team members:

- Rod Iwashita, Chief Harbor Engineer, Port of San Francisco
- Demetri Amaro, Commercial Property Manager for Fisherman's Wharf, Port of San Francisco
- Amarnath Kasalanati, PEER
- Mohammadreza Eslami, PEER–Hinman

At this meeting, an overview of the fire was provided by Rod Iwashita. Following the site visit and data collection, structural drawings and post-earthquake retrofit information were provided by the Port of San Francisco. The research team was provided with floor plans, elevation drawings, structural details, the post-Loma Prieta earthquake repair plan, and electrical drawings, in addition to schematics of the fire alarm system.

An internet-based database has been established by PEER to collect and archive this data as background for use in future fires and the resulting structural collapse. PEER's primary goal in establishing this database is to ensure that: (1) this data will be available for the research team to use in follow-up analyses of the fire and structural collapse; and (2) this data becomes a publicly-available resource for fire and structures researchers outside of this team to use in future analyses A secondary aim of PEER was to establish a database that is the foundation for an international database for significant building fire events where data can be captured and saved for the purpose of scientific research and investigation on the fire performance of buildings [Schulthess et al. [2020], Scawthorn [2011a,b]].

1.4 LAYOUT OF REPORT

The following is an overview of the general contents of sections contained in this report. The purpose of this preliminary reconnaissance report is to provide: (1) an overview of the fire hazard characteristics; and (2) to summarize the preliminary reports of damage to Pier 45. The lessons distilled from this information are presented in sections as follows:

Chapter 1: Introduction. This section provides an overview of the fire that started during the early hours of May 23, 2020, in the historic Fisherman's Wharf neighborhood of San Francisco. It also contains a review on past fire reconnaissance reports. Common techniques of fire reconnaissance are also introduced.

Chapter 2: General Overview of Pier 45. This section provides general characteristics and description of the building. This also explains the steps and approaches taken in the reconnaissance study.

Chapter 3: Description of the Structural System. This section provides information about the structural framing of Shed C, i.e., column sections, trusses, and connection details.

Chapter 4: Damage Levels. This section discusses the damage levels to structural elements such as columns, beams, and the timber roof, as well as nonstructural elements such as windows. It also discusses the mechanism of collapse based on the observations of the damage to structural elements.

Chapter 5: Preliminary Analysis. This section provides a preliminary structural fire analysis. Three different approaches for estimating gas temperature–time history are presented. The methodology for evaluating fire resistance is discussed.

Chapter 6: Conclusions and Future Directions. This section provides a summary of findings and lessons from the fire-induced collapse of Pier 45. Future directions based on vulnerabilities discovered through the reconnaissance effort are also discussed.

2 General Overview

2.1 LOCATION AND BUILDING CHARACTERISTICS

The historic Fisherman's Wharf neighborhood is a popular tourist attraction in San Francisco, California. It roughly encompasses the northern waterfront area from the Ghirardelli Square or Van Ness Avenue east to Pier 35. The massive fire on Pier 45 on Fisherman's Wharf on Saturday, May 23, 2020, caused extensive damage inside the building and destroyed the entire structure of Storage Shed C. The structure was initially built in 1926 as a part of the fisherman's wharf area in the Port of San Francisco. Later, following the 1989 Loma Prieta, California, earthquake, a seismic retrofit was performed, and bracing members were added to the main building as a part of lateral load resisting system.

The location of Pier 45 and the extent of fire is shown in Figure 2.1. The building was used by local fishermen to store equipment and process fish, including the region's annual Dungeness crab harvest. Approximately 7000 crab traps, 2000 shrimp traps, and 500 black cod traps were stored in this shed and were destroyed by the fire. These numbers could have been even higher as the shed was being re-purposed as a storage facility at the time of the blaze [Rubenstein and Kroichick [2020]].

An aerial view of Pier 45 prior to fire exposure is shown in Figure 2.2. The pier houses four sheds, each with direct access to water and road transportation. Sheds A, B, and D were not damaged by the fire. Shed C was most impacted by the fire. Shed C included office spaces for the Red and White fleet, storage areas for the SS Jeremiah O'Brien ship, and a fishing storage area for thirty tenants. Aerial view of Pier 45 after fire exposure showing the extent of damage is shown in Figure 2.3. Moreover, Figure 2.4 shows a side-by-side comparison before and after fire exposure of Pier 45.

Figure 2.5 shows fishing equipment piled outside of Shed C. Note: large amounts of fishing equipment similar to what is shown in Figure 2.5 may have served as fuel for the fire. Figure 2.6 shows the type of equipment being housed in Shed A, which is identical equipment that had been stored in Shed C. The historic SS Jeremiah O'Brien ship was spared from the fire, and it was towed to Pier 35 the Tuesday afternoon after the fire.

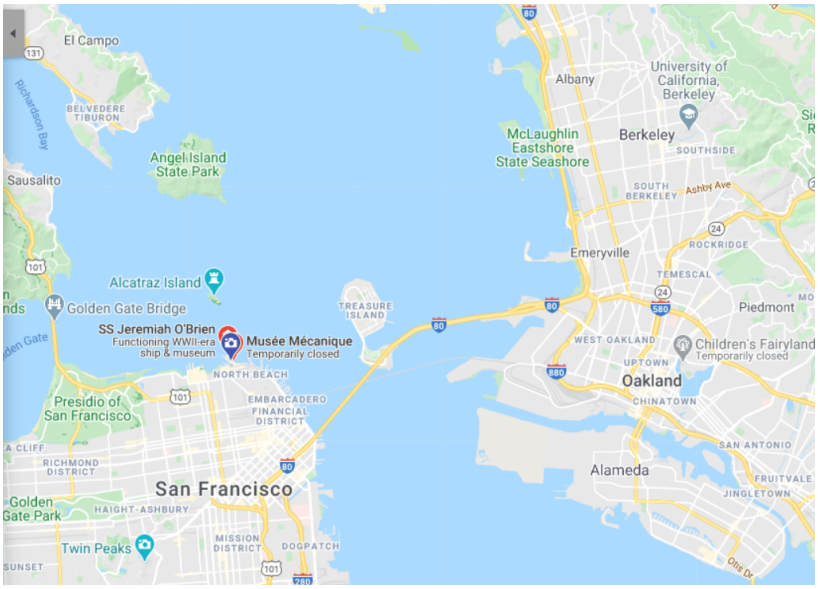

(a)

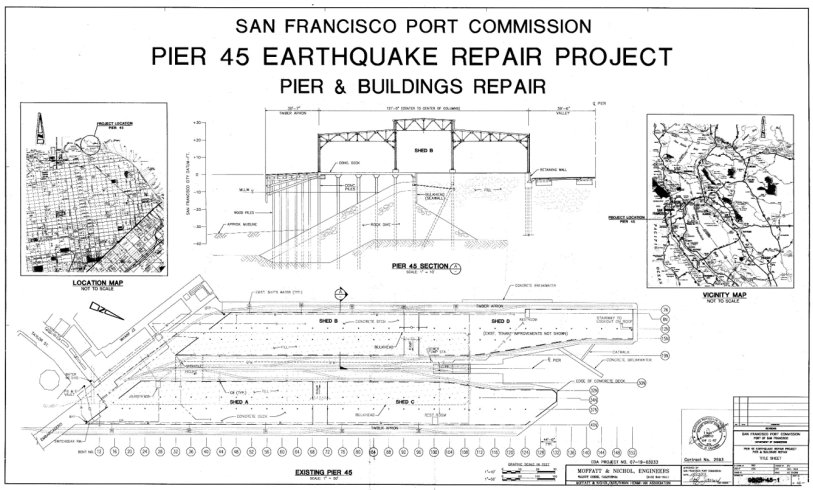

(b)

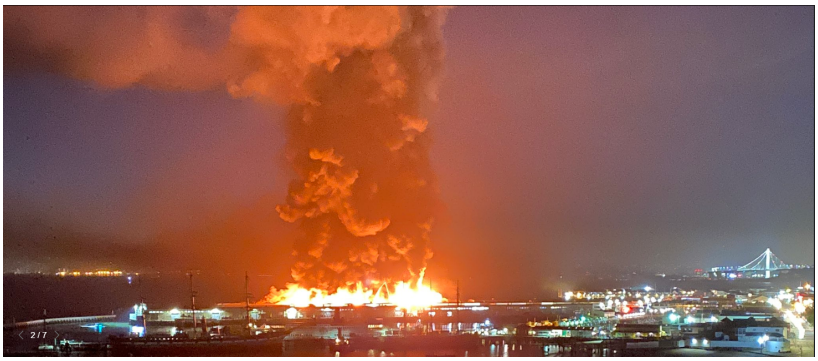

(c)

Figure 2.1: (a) Location of Pier 45 in the northern quadrant of the city (Credit: Google Earth); (b) sketch showing Pier 45 and Sheds A, B, C, and D; and (c) visible flames and smoke from this fire (Credit: Dan Whaley/AP Photo).

Figure 2.2: Aerial view of Pier 45 depicting sheds A, B, C, and D prior to fire exposure. The area affected by the fire, Shed C, is highlighted in yellow, along with the exposed perimeter of SS Jeremiah O'Brien highlighted in red.

Figure 2.3: Aerial view of Pier 45 showing extend of damage following the fire exposure. (Credit: CBS SF Bay Area, Nathan Wilde)

Figure 2.4: Aerial view of side-by-side comparison before and after fire exposure of Pier 45. (Credit: by ABC 7 News)

Figure 2.5: Large amounts of fishing equipment in front of Shed C.

(a) (b)

Figure 2.6: Passageway in Shed A: (a) fishing equipment; and (b) Shed A is identical in construction to Shed C.

2.2 RECONNAISSANCE EFFORT

The post-fire reconnaissance effort to study structural response under fire behavior can be broadly classified into three steps:

1. Collecting pre-fire and trans-fire structural information via design documents and visual observation;

2. Correlating structural and non-structural damage (failure) observations to fire severity; and
3. Qualitative and quantitative assessment of structural fire performance via prescriptive and/or performance based methods.

Accordingly, key information on compartment geometry and structural details was collected from design documents, followed by a systematic reconnaissance of the structure following the fire incident. Visual observations deemed pertinent to structural fire behavior were recorded through photos. An illustration of the general path while taking reconnaissance photos is shown schematically in Figure 2.7. This information was then used to correlate the extent of fire-induced damage (failure) to fire severity, providing data for a qualitative and quantitative assessment of structural fire performance. Both prescriptive guidance, and performance-based fire engineering design from first principles of fire severity (combustion of fuel), heat transfer, and thermo-mechanical structural response were applied to study damage and collapse of Shed C, Pier 45, San Francisco Fisherman's Wharf due to the massive fire that occurred on May 23, 2020.

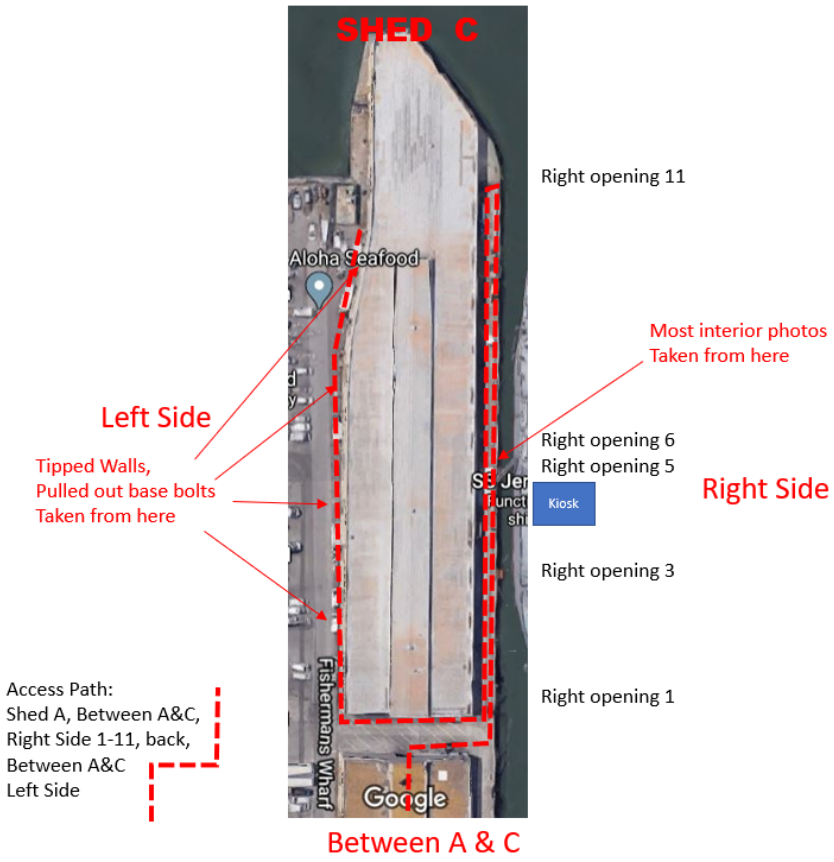

Figure 2.7: Schematic illustration of the walk-through path taken for collecting photographs during reconnaissance.

3 Description of the Structural System

The structure comprising collapsed Shed C, Pier 45, was built in 1928 with a seismic retrofit conducted in 1994. Drawings of both phases of construction are included in Appendix A. Figure 3.1 shows the layout of Pier 45, Shed C. The structural framing in Shed C was composed of a regular array of 15 bays of steel columns supporting a timber roof through a combination of trusses and wide flange steel beams, as shown in Figures 3.2 to 3.6.

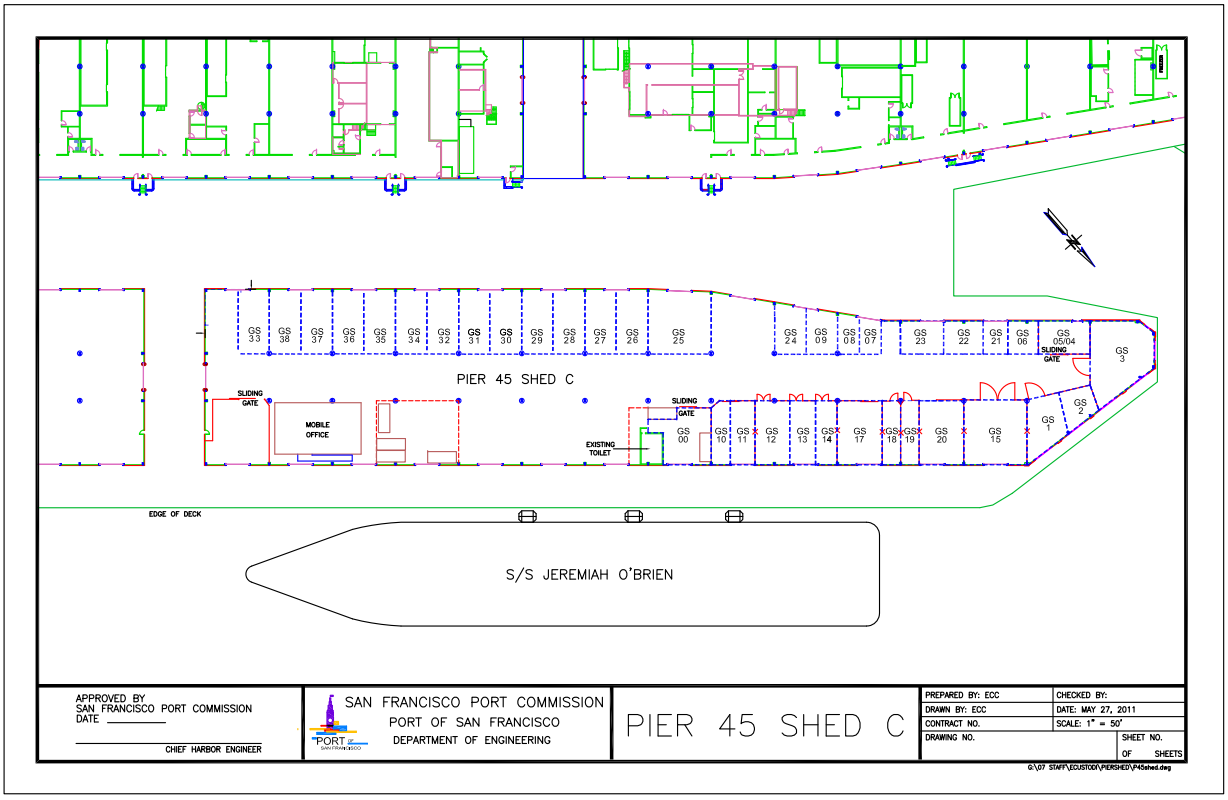

Figure 3.1: Pier 45 and layout of Shed C.

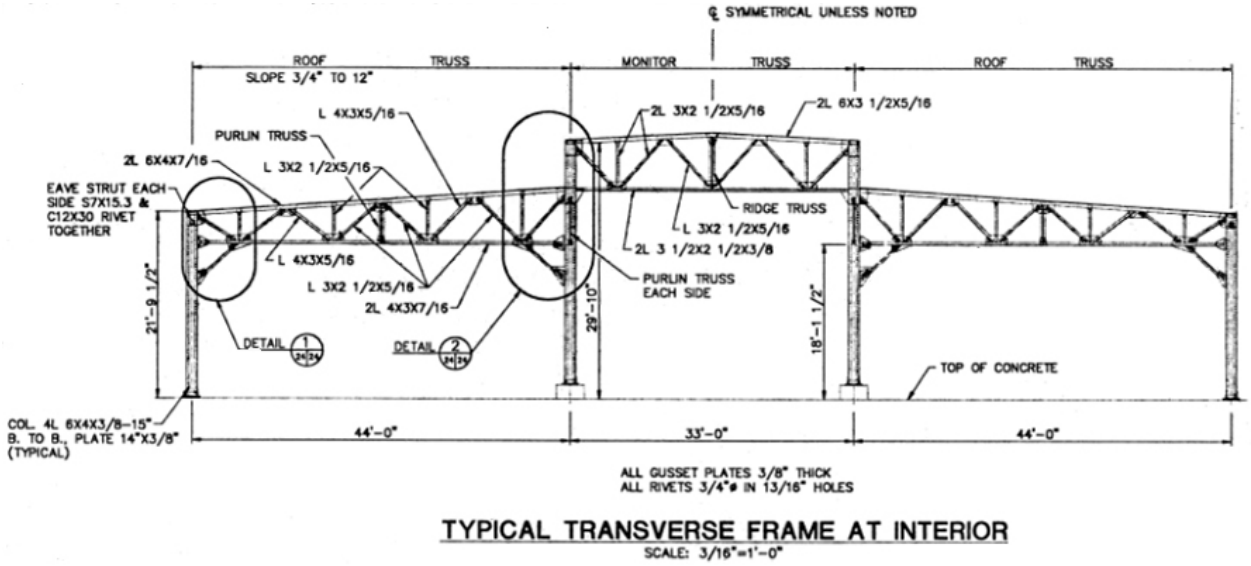

Figure 3.2: Typical transverse frame at interior part of Shed C.

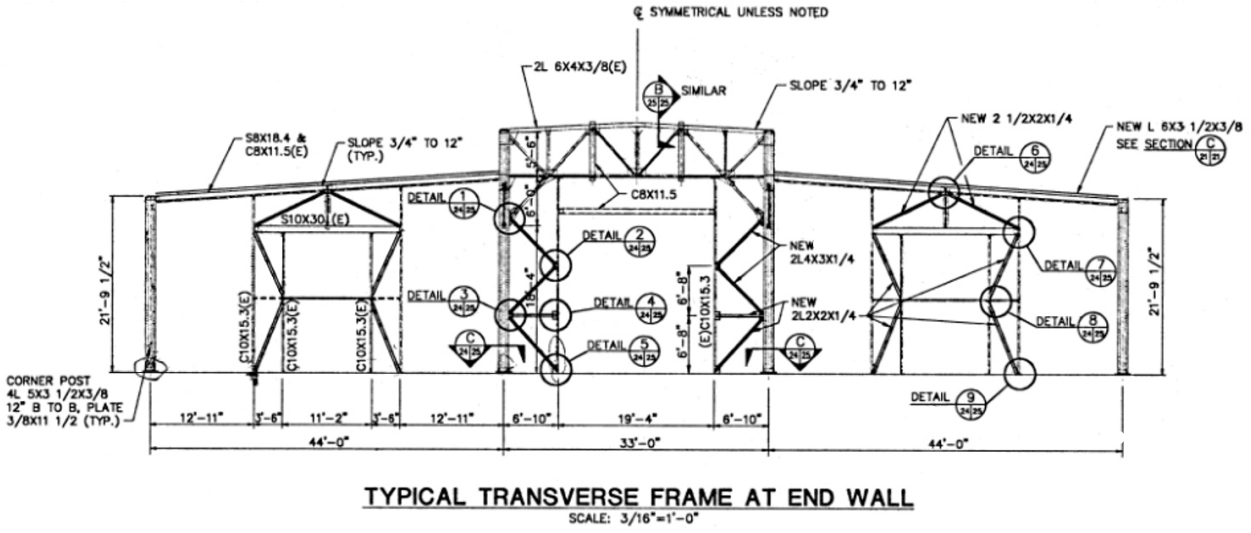

Figure 3.3: Typical transverse frame at end wall.

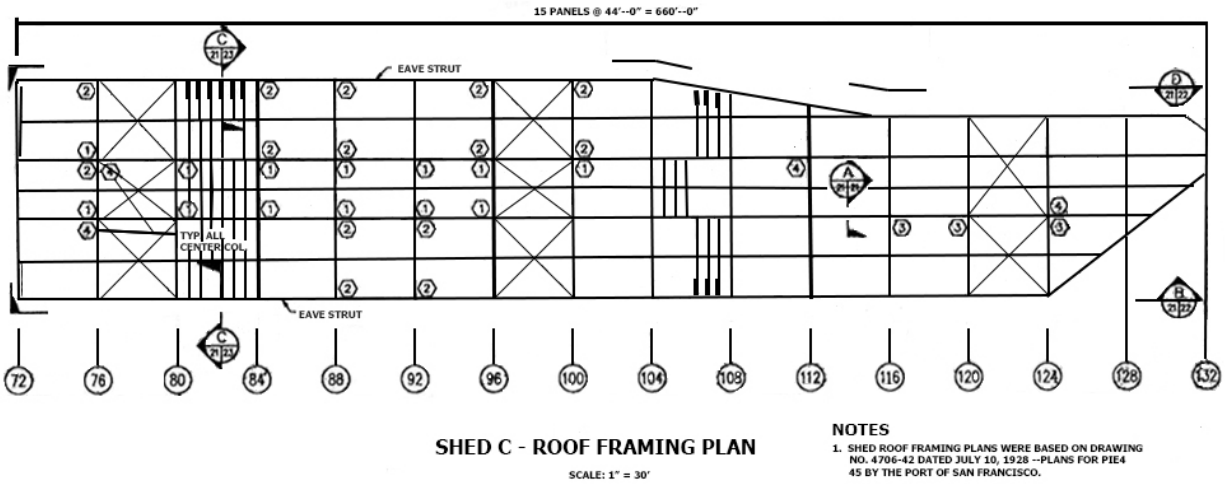

Figure 3.4: Shed C roof framing plan [sheet 9912-45-1 (21 0f 46)].

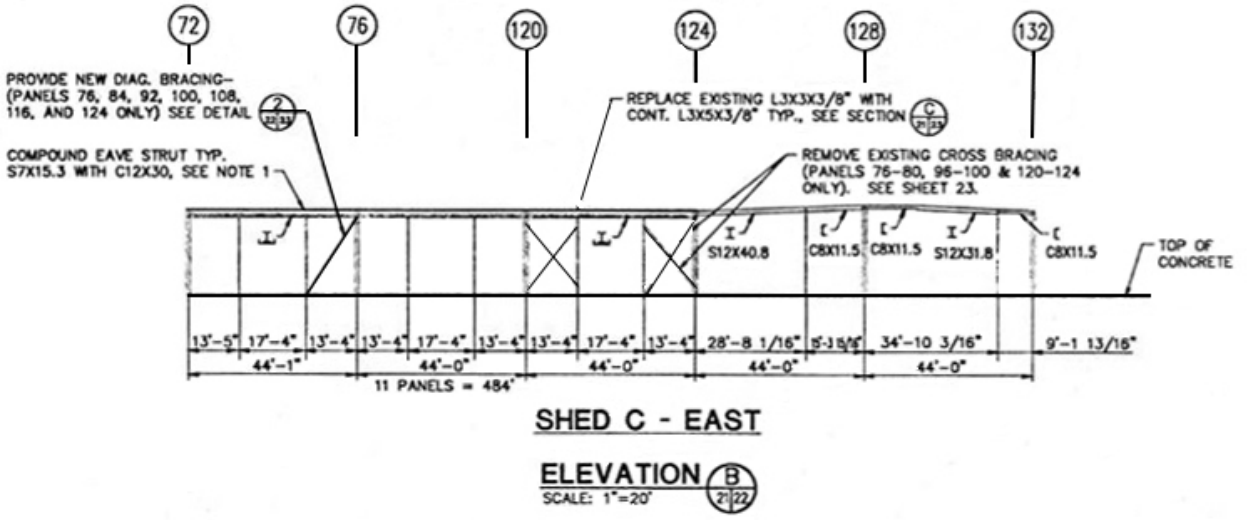

Figure 3.5: Shed C spans and retrofit installed in the east direction.

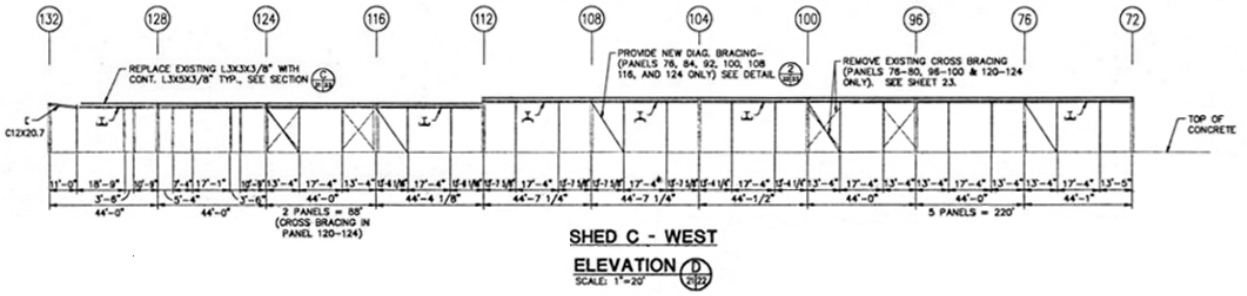

Figure 3.6: Shed C spans and retrofit installed in the west direction.

The columns consisted of built-up sections composed of four angle sections connected to two web plates via rivets. The columns were connected to the floor with a combination of base plates and anchor bolts, as depicted in Figure 3.7. The trusses were also composed of channel sections connected via rivets.

Connections between various structural elements were composed of gusset plates connected via rivets, bolts, and welds to base plates and channels. A typical transverse frame at the interior part of Shed C is shown in Figure 3.2. Details of truss to column connections is shown in Figure 3.8. The bottom chord was composed of 2L 4×3×7/16 steel channels; the top chord measured 2L 4×3×7/16. The truss web members measured L 4×3×5/16 and L 3×2-1/2×5/16. All dimensions of these cross-sections of the different steel members are in units of inches. A sample of the bottom chord detail is shown in Figure 3.9. These members were connected together by gusset plates via rivets.

Large windows (skylights) to allow for natural lighting were covered with tempered glass. Figure 3.10 shows the general structural system prior to fire exposure. The passageway in Shed C depicts primary structural framing, including columns, roof trusses, and W-shaped beams. A close-up view of undamaged condition of the truss and roof in Shed A is shown in Figure 3.11. The damaged condition of Shed C after the fire is shown in Figure 3.12.

Figure 3.7: Steel columns consisted of built up sections, composed of four angle sections connected with two web plates via rivets.

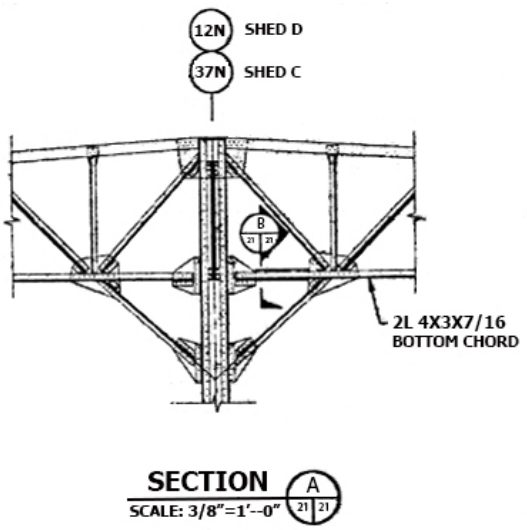

(a) Typical connection

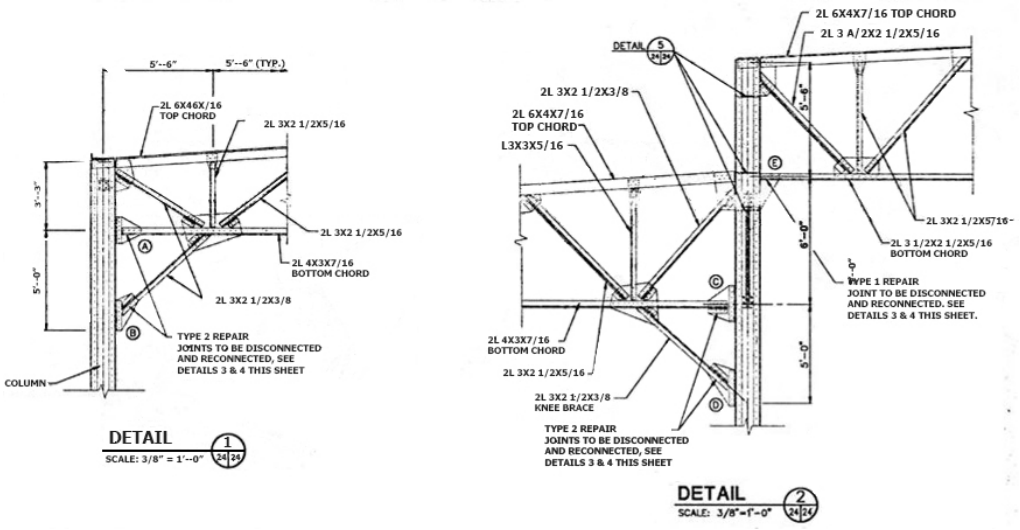

(b) Detail 1 and 2 for truss to interior/exterior columns

Figure 3.8: Details of truss to column connections: (a) typical connection; and (b) detail 1 and 2 for truss to interior/exterior columns.

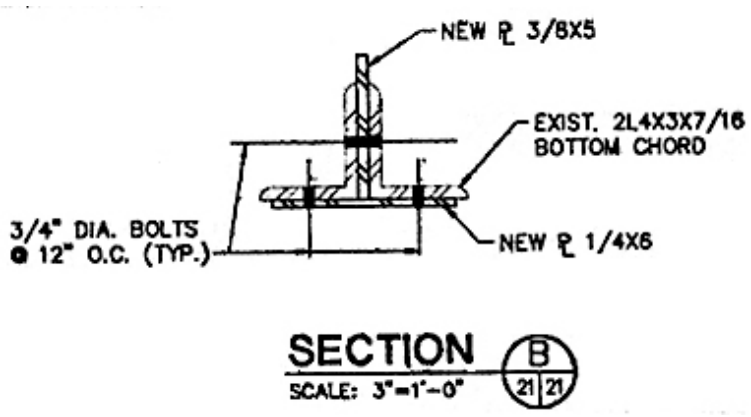

Figure 3.9: Bottom chord detail.

Figure 3.10: This photograph of the passageway in Shed A shows the general structural system in Shed C prior to fire exposure, i.e., the primary structural framing including columns, roof trusses, and W-shaped beams.

Figure 3.11: Undamaged condition of truss and roof of Shed A.

Figure 3.12: Damaged condition of Shed C from the the west-side view.

4 Fire Description and Structural Damage Observations

This chapter summarizes key observations from the reconnaissance efforts by providing a brief description of the fire, which is followed by damage observed in structural and non-structural members. Photographic evidence was collected to characterize temperature-induced damage to structural members (including concrete walls), connection performance, charring of the timber roof, damage to window glazing, and fire-induced collapse in major portions of the structure, with the exception of the northern part of the structure that did not experience major damage.

4.1 DESCRIPTION OF THE FIRE

The fire in Shed C was reported at around 4:15 am on May 23, 2020. The fire was fully developed and had attained flashover by the time firefighters arrived on scene, forcing the fire-fighting efforts to be defensive from the very beginning [Rubenstein and Kroichick [2020]]. The origin of the fire remains unknown at the time of writing of this Report. After initiation of fire, it is believed that large amounts of fishing equipment stored in Shed C were most likely the primary fuel load during the fire; see Figures 2.5 and 2.6, . In addition, at least two propane powered forklifts and a vehicle parked in the shed at the time of the fire added to the intensity of the fire. The four-alarm fire was brought under control almost seven hours later (around 11:30 am) through a significant fire-fighting effort involving 50 fire engines and 150 firefighters [Rubenstein and Kroichick [2020]]. Besides preventing fire spread to adjacent structures, protecting the SS Jeremiah O'Brien moored approximately 50 ft away from the burning structure was a key objective of the fire-fighting efforts. A fireboat producing streams of about 18,000 gallons of bay water per minute [Nolte [2020]] prevented significant damage to the vessel from the radiative and convective effects of the fire engulfing Shed C. A schematic illustration showing variation in heat release rate of uncontrolled fires in typical single-story industrial structures is shown in Figure 4.1 [Buchanan and Abu [2017]].

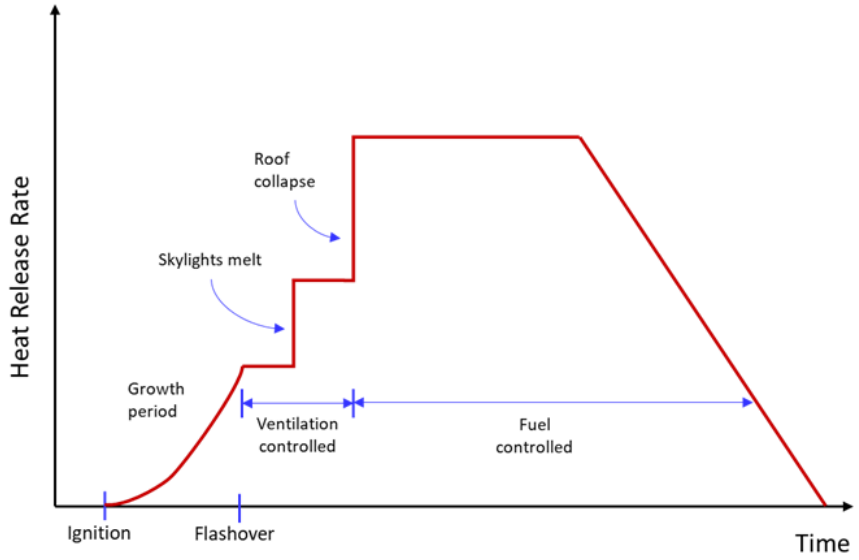

Figure 4.1: Illustration of heat release rate during a complete fire event in an industrial building.

4.2 GENERAL OBSERVATIONS

The concrete walls surrounding Shed C were connected to the steel columns by anchor bolts along the height of column. In turn, the column base plates were attached to the concrete base by anchor bolts. As a result of the fire, the east-side wall suffered extensive damage and began to incline inward; see Figures 4.2 and 4.3. The west side of the wall had completely collapsed inward, as shown in Figure 4.4. Figure 4.5 provides a more detailed look of the west side of the collapsed concrete wall.

The difference in the failure mechanisms of the eastern versus western concrete walls is explained in Section 4.3. Most of the observations were made from the perimeter of the building. A few areas on the east side of the structures were deemed safe enough to access the interior to conduct a visual inspection of the beams, connections, charred timber, and window glazing. Interior columns were observed from outside the structure because of safety concerns.

Figure 4.2: Damage on the east-side perimeter concrete walls and exterior columns.

Figure 4.3: Inward deformation of the built-up steel column and concrete wall on the eastern side of the structure.

Figure 4.4: Overturning of the columns supporting perimeter walls on the western side of the structure.

Figure 4.5: Failure of perimeter walls on the western side of the structure.

4.3 DAMAGE TO COLUMNS

Elevated temperature exposure during fire may cause a loss in the strength and stiffness in steel columns, resulting in a reduction of their load carrying capacity. Such reductions will eventually lead to collapse under normal service (gravity) loading. Prescriptive approaches typically imply a global failure (or critical) temperature of approximately 550°C for steel columns. Given the severity of the fire and lack of any passive fire protection (i.e., sprinklers), this temperature was conceivably attained in the columns within early phases of fire exposure. In addition to the critical temperature loads experienced by the columns, slenderness ratios and thermal gradients experienced during fire should be taken in account. Consequently, the fire-exposed columns exhibited distinct failure modes due to varying thermal and structural conditions that existed during fire exposure. Observed failure modes in the columns could be broadly categorized into two distinct groups, depending on their location in the structure:

1. Material yielding and local buckling in central and eastern columns, and
2. Global failure due to rupture of base plates and anchor bolts in the columns located at the western end of the structure.

At ambient conditions, slenderness ratio governs the yielding and/or buckling behavior of columns. Short columns with a slenderness ratio less than 50 fail through yielding or local buckling when the cross section comprising the plate elements have a high breadth-to-thickness ratios. Alternatively, long columns (with a slenderness ratio in excess of 100) tend to fail through classical Euler buckling. These general behaviors persist at elevated temperatures as well, but columns with different slenderness ratios lose capacity at significantly different rates with increasing temperatures. For instance, critical temperature for stocky and very slender columns can be about 500°C but can be as low as 300°C for columns with intermediate slenderness ratios.

The slenderness ratios for the columns in Shed C varied between 60 to 120, implying they were in the intermediate range, which typically experience greater rates of capacity reduction with increasing temperatures. Furthermore, the flange width to web depth of the cross section was approximately 0.86, while the width to thickness ratios of the flange varied between 26 to 32. These ratios represent a rather stocky cross section. That said, local buckling at the mid-height of the columns is clearly evident, as shown in Figure 4.6, indicating a more significant loss in local buckling strength compared to yield strength with increasing temperatures. It is also important to note that the built-up cross sections maintained their integrity throughout the fire exposure with no rupture observed in the rivets connecting the angle sections to the web plate.

(a)

(b)

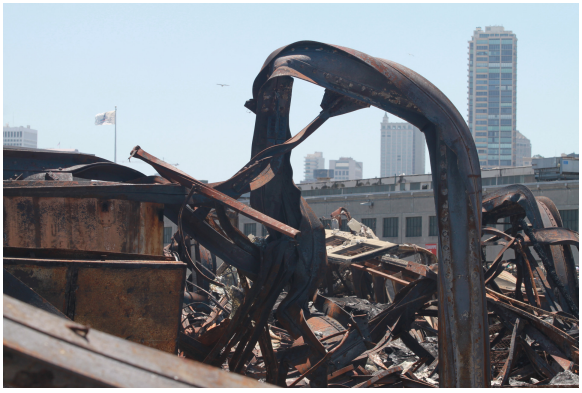

(c)

Figure 4.6: Damage in the middle part of a column on the eastern side of the structure: (a) typical middle column failure; (b) close-up view of middle column failure; and (c) typical column failure on the eastern side of the structure.

The second type of failure observed in the columns located on the western side of the structure occurred due to rupture and/or pull-out of anchor bolts that connected the base plates to the foundation, which occurred prior to capacity-based failure of the column. Such failure is a possible consequence of large overturning moments resulting from collapse of the interior columns, causing an asymmetrical increase in the tributary roof area transferred to the columns. The eccentric loads resulted in a large moment towards the inner part of the structure, causing the outer base plate anchors to fail in tension. Figure 4.7 shown a typical west wall pull-out and failure in the anchor bolts at a $45°$ angle in the anchor bolt body.

Furthermore, in cases where rupture of anchor bolts did not occur, bowing and failure of the perimeter concrete wall at the foundation resulted in collapse of the columns. This was possibly due to severe corrosion at the foundation of the perimeter wall; see Figure 4.8. This corrosion occurred due to the presence of drainage pipes, coupled with adverse conditions from the maritime environment; see Figure 4.9. It is worth noting that the design and construction techniques typical of the 1920s may have contributed to the failure. Figure 4.8 indicates a very shallow anchorage, and it is not clear if the failure was due to corrosion or the lack of anchorage at the column bases

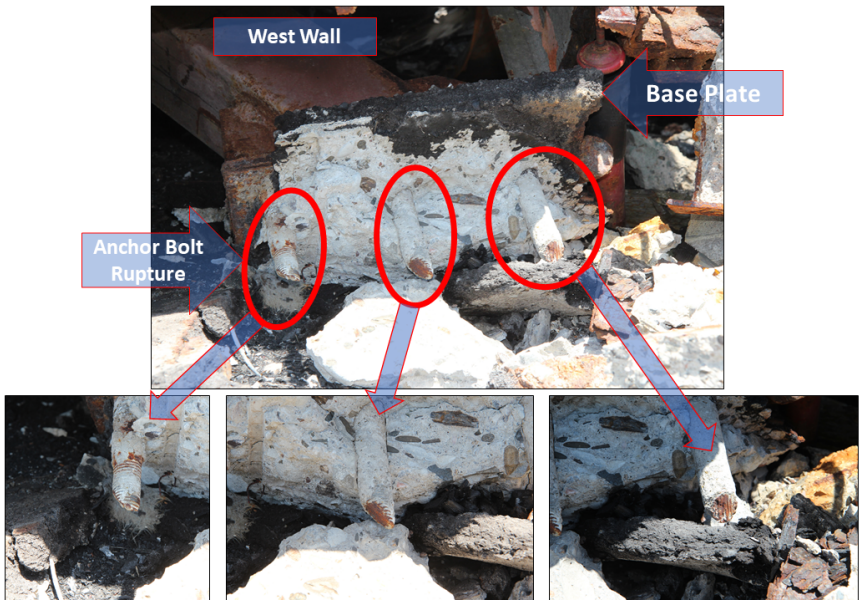

Figure 4.7: Pull-out and rupture in the anchor bolts at a $45°$ angle.

Figure 4.8: Failure of perimeter walls on the western part of the structure.

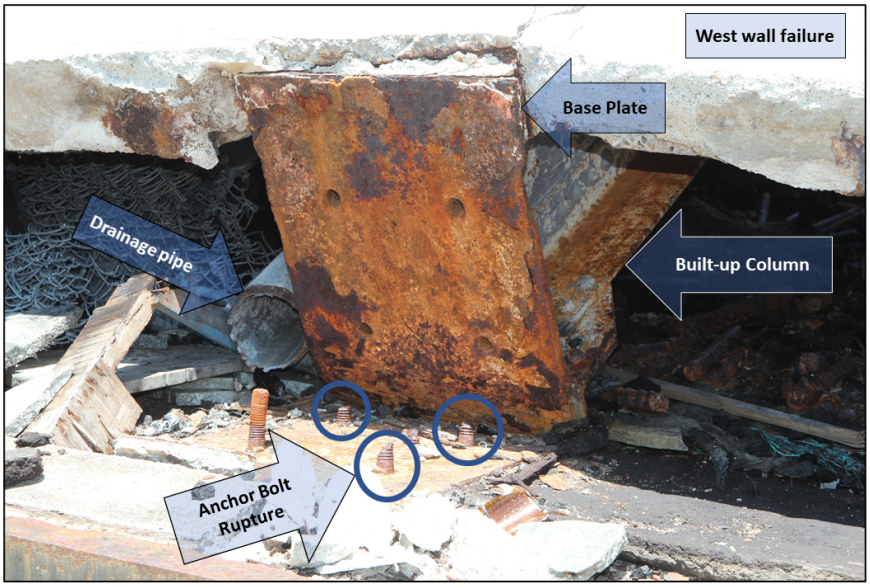

Figure 4.9: Typical pull-out and failure mechanism in the anchor bolts in the west wall.

4.4 DAMAGE TO BEAMS AND ROOF TRUSSES

The horizontal framing members failed completely in major portions of the structure. Temperature-induced damage to the trusses and beams supporting the roof can be categorized into two broad categories:

1. Excessive in-plane deflection due to loss in strength and stiffness; and
2. Significant out-of plane deflection due to buckling and twisting.

Significant sagging was observed especially in the mid-span of horizontal framing members due to loss of strength and stiffness from temperature-induced degradation in the mechanical properties of structural steel. The extent of mid-span deflection varied significantly for similar members, owing to large spatio-temporal variability in gas temperatures experienced within Shed C. This variability can also be partly attributed to failure of columns prior to failure of beams and vice-a-versa.

Besides excessive in-plane deflection, significant out-of-plane deflections were also evident in the beams; see Figures 4.10 and 4.11. This indicates the presence of significant fire-induced restraint forces in the beam that developed during fire exposure, transforming its behavior to that of a beam–column. The response of such restrained steel beams (or beam–columns) under fire depends on many factors, including: the specific fire scenario, beam slenderness ratio, location of axial restraint at the supports, and high-temperature properties of steel [Eslami et al. [2018], Kodur et al. [2017], Anvari et al. [2019]].

Figure 4.10: Significant out-of-plane deformation in collapsed beams.

Figure 4.11: Close-up view of out-of-plane deformations in the beam from thermal gradients and restrained thermal expansion.

4.5 CONNECTION PERFORMANCE

As noted in Section 4.3, the steel column to concrete base connection on the west side of the building failed in numerous ways . This section focuses on the truss-to-column connections. While the top chord, bottom chord, and web members suffered significant fire-induced damage, the connections were found to be relatively intact during the site visit, suggesting adequate performance during fire exposure. There were no records of gusset plate rupture, rivet failure, or block shear failure. This confirms the design concept that the connection may fail after the full capacity of the connecting members is achieved. Figure 4.12 shows samples of damage to truss connections. While excessive deformation of gusset plates can be seen in Figure 4.12, there was no evidence of block shear or rivet failure in the connecting members.

(a)

(b)

Figure 4.12: Damage to truss connection: (a) excessive deformation in truss members with no failure in rivet or gusset plate; and (b) typical truss connection exhibiting severe deformation and collapsed connection members.

4.6 DAMAGE TO TIMBER ROOF

The timber roof was connected to the steel members by stud bolts. Total failure of the timber roof was observed over the entire building. Figures A.4 and A.5 shows samples of timber roof charring of the east side of Shed C. Wood is a combustible material and experiences charring when exposed to fire. Loss of structural integrity due to charring represents the primary mode of failure

in structural wood elements. Severe charring and complete burning of wood occurred at many locations, especially in the central part of Shed C. Relatively moderate charring was observed in the roof close to the perimeter walls.

The thermal analysis of timber members requires special consideration of the thermal decomposition of wood under heating. Thermal decomposition begins with a moving pyrolysis front that transforms the wood to char through a process that results in mass loss, discoloration, and the emission of gaseous byproducts [Buchanan and Abu [2017]]. Knowledge of the char extent is required for proper thermal analyses because the thermal properties of charred wood are significantly different from those of uncharred wood [Committee [2018]]. Hence, further study is needed to analyze the expected level of charring as part of a thermal response analysis. Char develops between 536°F (280°C) and 608°F (320°C), with a temperature of 550°F (288°C) typically used in locating the pyrolysis front using embedded thermocouples [White].

Under standard fire exposure, the pyrolysis front moves at a fairly constant rate after approximately 45 minutes. Although the rate of charring is effectively nonlinear because of the insulating effect of the char layer, the charring rate at one hour under a standard fire exposure is often used as the nominal char rate and is used as the reference char rate in nonlinear charring models, such as those used in the National Design Specification for Wood Construction [Council [2012]]. It is recommended to measure the moisture content in Shed A, as it is identical to Shed C, to evaluate the char rate in Shed C [Babrauskas [2005]]. Other factors such as wood species, density, orientation of grain, and inherent variability of wood as a natural material have less influence on the moisture content; however, it is recommended to obtain some specimens prior to the demolition of Shed C to ensure that this timber is identical to that used in constructing Shed A.

Figure 4.13: Timber roof charring from the east side of the structure.

Figure 4.14: Completely burnt charring of the roof on the east side of the structure.

4.7 MILL SCALE AND FLOW IN STEEL MEMBERS

Besides structural failure, mill scale and signs of material flow (phase transformation) were evident on the the outer surfaces of steel beams and truss members. Figures 4.15 and 4.16 show severe mill-scale peeling on the flange of channel-section beams. The resultant morphology, microstructure, and phase transformation (composition) of fire-damaged steel is dependent on the oxidation characteristics and can be correlated to the elevated temperature experienced during the fire [Xie et al. [2018]].

Figure 4.15: Mill-scale and material-flow patterns had formed on the outer surfaces of a truss member.

Figure 4.16: Mill-scale peeling on the flange of channel-section beams.

4.8 DAMAGE TO WINDOW GLAZING

There were glass windows in the upper part of the perimeter walls of Shed C. Many of the window frames on the east side of the structure were distorted due to deformation in the concrete wall, causing severe cracks in the glass. In some parts of the structure, the glass had melted due to excessive heat; the molten glass was mostly located at the top of the openings. This matches with the direction of heat toward outside of the building, indicating that the glass at the top of openings underwent higher temperatures and eventually led to melting of the glass.

Published data shows that 550–600°C is the critical temperature for both fully tempered and heat-strengthened glass types. When the average furnace temperature is around 615°C, glass temperature reaches the critical temperature (550°C). The glass behavior changes to a plastic phase at the critical temperature. At this point, the glass is not solid anymore and behaves more like a liquid material, and it is not able to carry any loads, not even its self-weight [Nodehi [2016]].

Damage to glass can be seen in the Figures 4.17 to 4.22. It is recommended to conduct furnace tests on samples of undamaged glass of Shed C. Obtaining the melting temperature of glass can significantly help in estimating the actual temperature of the structure. In fact, glass can be used as evidence to evaluate the actual temperature of the Shed C fire [Lentini [1992]].

Figure 4.17: Damage to window and glass in east-side perimeter wall.

Figure 4.18: Damage to window frame and glass.

Figure 4.19: Damage to window frame and molten glass in the east wall.

Figure 4.20: Molten glass in the east wall.

Figure 4.21: Severe glass damage on the top of opening (left) vs. limited damage on the top of concrete wall (right).

Figure 4.22: Deformed glass in east side of the structure.

4.9 MECHANISM OF COLLAPSE

A simplistic sequence of events is hypothesized based on engineering judgment and information collected through the reconnaissance effort. The complex interrelated sequence of events that might have occurred are described as follows:

1. Elevated temperatures caused heating of horizontal members (beams and trusses) as they were exposed to rising hot gases, followed by an increase in temperature of columns as the fire spread across the structure;

2. A rapid increase in the temperature of the horizontal steel members resulted in outward thrust forces on the columns and perimeter walls during initial phases of fire exposure;

3. Temperature in the columns, especially in the middle part of the structure, increased rapidly, causing the columns to reach critical temperature.

4. Outward thrust forces from the horizontal members stabilized due to loss of member stiffness as temperatures increased further. Eventually, the horizontal members sagged into a catenary, transforming the outward thrust into in an inward tensile force;

5. As temperatures increased even more, failure of the middle columns occurred due to combined effects of applied load, thermal bowing, and local buckling. Collapse of some (or all) of the middle columns exacerbated the effects of the tensile forces of the horizontal members, resulting in large overturning moments on the perimeter columns and walls; and

6. The inward tensile force resulted in the observed overturning and failure of the perimeter columns leading to fire-induced progressive collapse of the structure. Strong foundations prevented such overturning on the east side to some degree, but the columns on the west side had a significantly weaker foundation and collapsed completely.

Clearly, the overall diaphragm stiffness of the structure was sufficient to prevent outward collapse of any of the perimeter columns or walls. This can be partly attributed to the post-Loma Prieta earthquake retrofit of the structure. The retrofit was critical in ensuring that the overall collapse of the structure was inward (towards the fire), despite any special provisions for fire design.

Early failure of the columns due to the lack of passive fire protection or design to resist the effects of fire resulted in progressive collapse of the structure. Thus, the significance of provisions for structural fire safety in this fire, especially in regards to the columns, is highlighted. More detailed studies are needed to verify this hypothesis and better understand factors that result in fire-induced progressive collapse of such buildings. Furthermore, numerical studies on characterizing fire severity and the progression of damage in structural and non-structural members can substantiate these observations to help reach a definitive explanation for the fire-induced collapse scenario that occurred in Shed C.

5 Preliminary Analysis

A preliminary structural fire analysis was conducted to qualify the observed failures modes and damage to Shed C. The analysis can be broken down into three key steps:

1. Estimation of gas temperature versus time to approximate fire environment;
2. Calculation of temperatures experienced within the structural member; and
3. Evaluation of the fire resistance of the members.

For the sake of simplicity, typical primary framing members i.e., steel columns and wide flange beams, were analyzed, assuming no load sharing (redundant behavior) or accounting for temperature-induced buckling and second-order effects. An overview of the methods used, input parameters, and results from preliminary analyses are presented below.

5.1 ESTIMATING GAS TEMPERATURE–TIME HISTORY

Several approaches are available to correlate the fire environment to a representative gas temperature–time relation, and can be broadly classified into three different categories based on increasing complexity as following:

- Standard fire relations
- Empirical compartment fire models
- Computational fluid dynamics (CFD) models

The first and most simple approach assumes a standard fire relation to represent the fire environment. These relations form the basis of establishing prescriptive fire resistance ratings used by building codes. Generally, a single relation represents all possible fire conditions, neglecting the effect of varying fuel load, ventilation conditions, compartment geometry, and duration of the fire. A simple approximation of the ASTM E119 relation is given by the following equation [Lie [1995]]:

$$T = 750 \left[1 - e^{-3.79553\sqrt{t_h}}\right] + 170.41\sqrt{t_h} + T_0 \tag{5.1}$$

where T represents gas temperature ($^{\circ}$C), t_h represents time (hours), and T_0 represents ambient temperature ($^{\circ}$C).

Alternatively, empirical compartment fire models can be applied to explicitly account for fuel load, ventilation conditions, compartment geometry, and fire duration. A number of published curves, zone models, analytical approaches, and empirical methods exist in published literature; however, given the large geometry of the compartment and limited information, the BFD curve proposed in [Barnett [2002]] is utilized in these preliminary calculations. The general form of which can be written as:

$$T = T_m e^{-z} + T_0 \tag{5.2}$$

where T_m represents the difference between peak fire temperature and ambient temperature, and z is a non-dimensional parameter given by:

$$z = \frac{(\ln t - \ln t_m)^2}{s_c} \tag{5.3}$$

where t represents time from ignition of fire (min), t_m represents the time to peak fire temperature from ignition (min), and s_c is a dimensionless shape constant.

Finally, the CFD provides the most realistic and accurate representation of the fire environment and can be implemented using a number of available computer program, such as Fire Dynamics Simulator (FDS). Such modeling is complex and requires significant technical and computational effort that is beyond the scope of this preliminary analysis.

5.2 CALCULATION OF CROSS-SECTIONAL TEMPERATURE

Once the temperature–time relationship during fire exposure is known, one can calculate the temperatures within the steel cross section. The rate of temperature increase within steel members is governed by the ratio of heated perimeter to the mass of the member, density, thermal conductivity, and specific heat of steel. A lumped heat capacity method proposed by Buchanan and Abu (2017) is applied to calculate temperature progression in unprotected steel members. The increase in steel temperature as a function of fire temperature and time can be calculated using the following equation:

$$\Delta T_s = \frac{F}{V}\frac{1}{\rho_s c_s}\left[h_c(T_f - T_s) + \sigma\epsilon(T_f^4 - T_s^4)\right]\Delta t \tag{5.4}$$

where, T_s represents the temperature of steel ($^{\circ}$C), F represents the surface area of the exposed member (m^2), V represents volume of unit length of the member (m^3), ρ_s is the density of steel, c_s is the specific heat of steel, h_c represents the convective heat transfer coefficient (W/m^2K), T_f represents average fire temperature at half time step ($^{\circ}$C), σ is the Stefan-Boltzmann constant ($5.67 \times 10^{-}11\ kW/m^2K^4$), ϵ is the resultant emissivity (dimensionless), and Δt represents the

incremental time step (s). Note that this approach assumes the cross section to be a lumped mass at uniform temperature, thereby ignoring variation resulting from heat conduction within the cross section.

5.3 METHODOLOGY FOR EVALUATING FIRE RESISTANCE

The fire resistance of a structural member can be defined as its ability to resist failure as per insulation, integrity, and/or load bearing criteria for a given fire scenario (severity). The fire resistance of a member capable of exceeding the severity of a given fire scenario can be computed in the time domain, temperature domain, or the strength domain. For this study, fire resistance calculations in the temperature domain were considered for simplicity. As per this method, a member is said to survive the fire exposure if the critical temperature (temperature beyond which a member is expected to fail) is greater than or equal to the maximum temperature experienced by the member for a given fire scenario, i.e.,

$$T_{crit} \geqslant T_{max} \tag{5.5}$$

where, T_{crit} represents critical temperature beyond which failure is expected ($^{\circ}$C), and T_{max} represents the maximum temperature in the element for a given fire scenario calculated through heat transfer or specified at a time prescribed by a building code ($^{\circ}$C).

Critical temperature for a member fabricated using carbon steel for a uniform temperature distribution and a given load ratio (or degree of utilization) can be computed per the following expression [for Standardization [CEN]]:

$$T_{crit} = 39.19 \ln \left[\frac{1}{0.9674\, r_0^{3.833}} - 1 \right] + 482 \tag{5.6}$$

where, r_0 represents the load ratio of the member defined as the ratio of the ultimate capacity at room temperature to the applied load during fire exposure (dimensionless).

Although relatively simple to apply, it is crucial to note that calculations of fire resistance in the temperature domain are generally not recommended for load bearing structural members as they do not account for deformation criteria or instability phenomena arising from thermal gradients. Nonetheless, since the goal of this analysis is to quantify the possible failure mechanism leading to fire-induced collapse, it was deemed applicable in the present study.

5.4 INPUT PARAMETERS FOR ANALYSIS

Different input parameters including details of the geometric cross section, load ratio, and material properties were determined based on available information and engineering judgement. As discussed below, these parameters can be broadly categorized as they relate to fire severity and heat transfer, as well as the properties of the members themselves.

Table 5.1: Input parameters to generate baseline BFD curves.

Designation	T_m (°C)	t_m(min)	s_c(dimensionless)
SF	1260	19	1.9
LF	740	115	4.5

5.4.1 Fire Severity and Heat Transfer

Three distinct fire scenarios were considered to calculate gas temperature–time curves representing the fire environment. The first scenario assumes the standard fire exposure per ASTM E119 calculated as a function of time. In addition, a short fire scenario (SF), and a long fire scenario (LF) calculated using BFD curves calibrated to large-scale Cardington tests [Kirby et al. [1999]] were chosen to represent a more realistic temperature-time history. The fitting parameters for Equation (5.2) described in Section 5.1—used to generate the time-temperature curves—are summarized in Table 5.1.

For simplicity's sake, the fitting parameters for the BFD curves used in this study are based on test data. The duration of fire exposure prior to ignition lasts for approximately one-and-one-half hours for SF, and seven hours for LF, corresponding to the upper-bound based on fire-fighting timeline. In addition, given that molten glass was observed during reconnaissance efforts, assuming peak fire temperatures in excess of 1200°C is reasonable [Lentini [1992]]. More accurate calculation of the actual fire temperatures based on realistic fuel loads and compartment characteristics is possible using this approach, but it requires more detailed assumptions and calculations beyond the scope of this preliminary study. The value of the convective heat transfer coefficient and resultant emissivity to model heat transfer from the fire to the structural member was assumed to be 25 W/m^2K and 0.5, respectively for Standardization [CEN].

5.4.2 Member Characteristics and Material Properties

The baseline collapse hypothesis is based on collapse of interior columns prior to failure of the wide flange beams (or roof trusses) and subsequent failure of the perimeter columns adjacent to the perimeter walls. Accordingly, a beam cross section and built-up column cross section were considered for temperature calculations. For simplicity, the sections were assumed to consist entirely of rectangular components. The assumed dimensions and calculated section factors, based on four-sided and three-sided exposure conditions, are summarized in Table 5.2. Here, D represents the overall depth of the section, B represents the overall width of the section, t_f represents the thickness of the flange, and t_w represents the thickness of the web.

Besides geometrical properties, we assume the physical and thermal properties of structural steel to calculate the temperature within the member. The density of steel is assumed to be 7850 kg/m^3, and the specific heat is assumed to be 600 J/kgK. Note that temperature-dependent variations in specific heat are ignored for simplicity.

Table 5.2: Idealized dimensions and section factors of steel members.

Shape	D(mm)	B(mm)	t_f(mm)	t_w(mm)	F/V(m^{-1})	
					3-sided	4-sided
S8×18.4	254	102	10.8	7.9	198	223
Built-up column	305	356	9.5	9.5	175	212

5.5 RESULTS AND DISCUSSION

Figure 5.1 plots the calculated temperature–time histories for the assumed fire scenarios along with temperature progression within the steel member cross sections for the first 180 minutes (or three hours) of fire exposure. The critical temperature calculated to be 585°C corresponding to a load ratio of 0.5 is also plotted to determine expected failure time based on the temperature criteria discussed in Section 5.3.

Clearly, the temperature progression in the cross sections follow the calculated gas temperatures for the respective fire scenarios. Moreover, variation in cross-sectional dimensions or exposure conditions seems to have negligible effect on the temperatures experienced within the member. In case of ASTM E119 fire exposure, temperatures increased monotonically, and the critical temperature was reached within 16–18 minutes into fire exposure. The time to reach critical temperature in the case of fire scenario SF with a greater rate of increase in temperature compared to ASTM E119 exposure occurred between 12 to 13 minutes for the considered cross sections. Finally, in the case of fire scenario LF, both the peak gas temperature and rate of temperature was significantly lower, and critical temperature was exceeded almost 47 to 50 minutes into fire exposure.

Therefore, it is postulated that the non-fire-rated steel members (the frame) failed during early phases of fire exposure once flash-over occurred. However, a more detailed analysis is needed to substantiate the complex sequence of interrelated events that led to fire-induced progressive collapse. As shown, results can vary significantly depending on assumptions regarding the fire scenario (gas temperature–time history). Further studies are needed to accurately represent the thermal environment that existed during fire exposure.

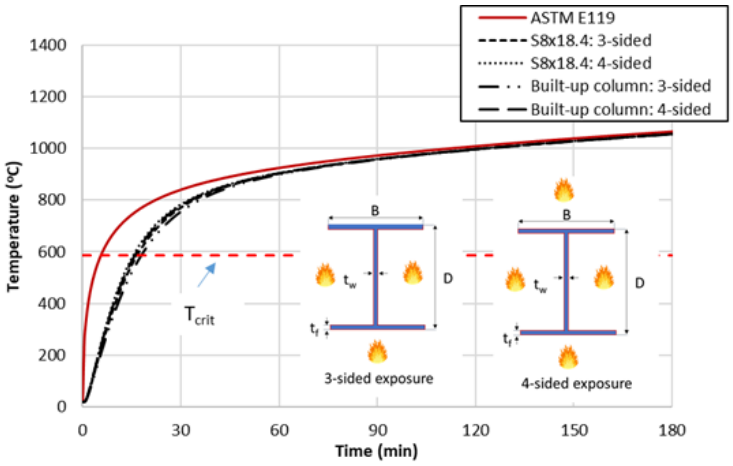

(a)

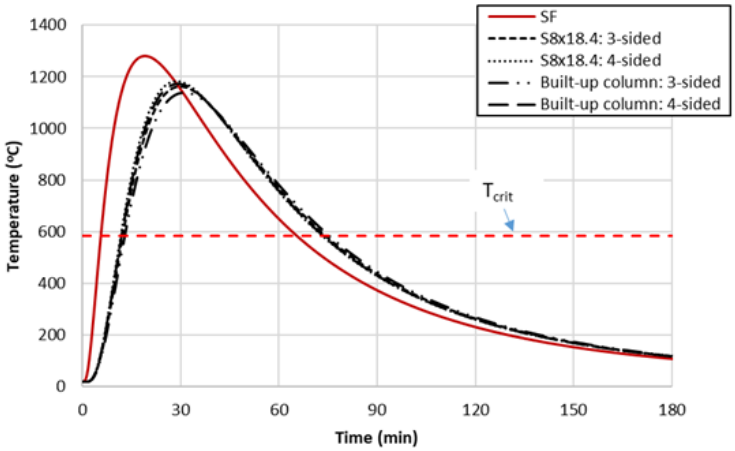

(b)

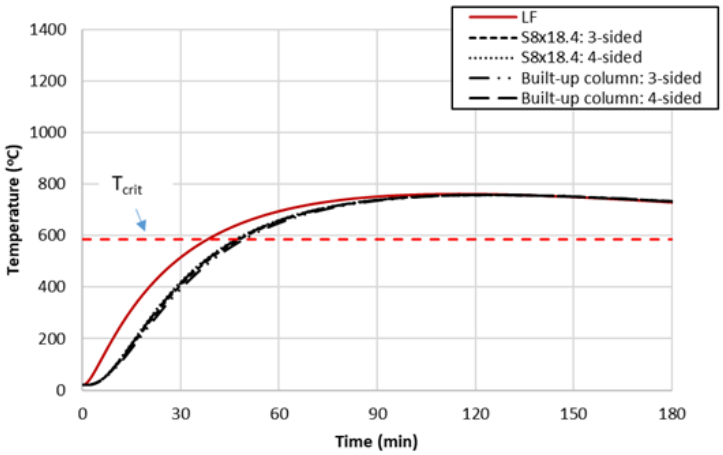

(c)

Figure 5.1: Calculated temperatures for different fire scenarios and exposure conditions: (a) temperature progression with time for ASTM E119 fire exposure; (b) temperature progression with time for SF fire exposure; and (c) temperature progression with time for LF fire exposure.

6 Conclusions and Future Directions

The fire of May 23, 2020, in Shed C at Pier located in the historic San Francisco Fisherman's Wharf neighborhood, provides a rare opportunity to learn from a fully developed large-compartment fire that caused fire-induced collapse of large portions of the structure. As noted in the fire incident reports, lack of effective passive compartmentation resulted in rapid fire spread in the central parts of the structure. While details pertaining to the origin and spread of the fire remain unknown, significant reduction in the load-bearing capacity of the columns in the central part of the structure may have triggered the sequence of events leading to structural collapse.

Based on engineering judgment, it is hypothesized that the columns failed before the horizontal framing members (beams or roof trusses) could achieve full capacity. In addition, preliminary analysis demonstrates that it was possible that the severity of the fire was sufficient for the non-fire-rated members to fail during early phases of fire exposure.

Worth noting is that the post-earthquake retrofit of the structure after the 1989 Loma Prieta, California, earthquake improved the lateral stability (diaphragm stiffness) of the structure, implicitly improving the overall fire-performance of the structure as it resulted in a more desirable inward collapse. Outward collapse of perimeter walls may have resulted in further fire spread, thus endangering firefighters. In addition, special design provisions for fire and/or passive fire protection in columns may have significantly enhanced the response of the structure during fire.

Lessons from this post-fire investigation highlight the need of adequate consideration of unique conditions that exist during fire. It may be prudent to make such considerations in conjunction with retrofit efforts made before or after earthquakes for aging structures. The fire-induced collapse of Shed C at Pier 45 shows that improving fire performance of columns can be crucial for fire safety and may not be achieved through seismic retrofits alone.

To better understand the fire severity and resulting damage to structural members, the following experimental program is being requested from the Port of San Francisco:

- Material tests on steel members
- Material tests on glass
- Material tests on timber roof panels
- Samples of typical materials stored in Shed C
- Humidity measurements from Shed A
- Material test on steel bolts and anchor rods

- Material tests on concrete from perimeter walls
- Material tests on reinforcing steel from perimeter walls

Results from these material tests, in conjunction with structural drawings provided by the Port of San Francisco for Shed C, will be used to develop a nonlinear multi-resolution multi-degree-of-freedom (MDOF) finite-element model using the general purpose software ABAQUS [Hibbitt et al. [2019]]. In particular, the material tests will be used to calibrate temperature-dependent material properties to capture the the complex inter-dependencies of structural systems and the progression of collapse under fire loading.

General observations and lessons learned through the reconnaissance efforts have highlighted the following vulnerabilities:

- The vulnerability of similar sheds in the Fisherman's Wharf area: nearby sheds are of similar construction, used for similar purposes, and store similar materials that are susceptible to fires of this nature.
- The vulnerability of buildings of this type: Shed C was nearly 100 years old and highlights the vulnerability of similar structures located in the City.
- The unknown performance of seismically retrofitted structures in fire: Shed C appears to have benefited from the improved lateral stability by exhibiting an inward collapse mechanism; it remains unclear if that was the design objective. Combining seismic retrofit strategies with improved fire protection would be a more holistic approach to risk reduction.
- The vulnerability to the City: This single four-alarm event required significant fire-fighting effort (50 fire engines and 150 firefighters) and raises questions about mitigation efforts for fires following earthquake, which can simultaneously occur at several locations in the City.

These vulnerabilities highlight future directions that can be taken to improve best practices in performance-based structural fire engineering and fire safety.

REFERENCES

S. Rubenstein and R. Kroichick. Early morning fire consumes warehouse on SF's fisherman's wharf. *San Francisco Chronicle*, 2020. https://www.sfchronicle.com/bayarea/article/Warehouse-fire-rages-at-Pier-45-on-Fisherman-s-15290787.php.

M. Cabanatuan and M. Cassidy. Huge fire near central freeway in SF spreads to multiple buildings, injures firefighter. *San Francisco Chronicle*, 2020. https://www.sfchronicle.com/bayarea/article/Early-morning-structure-fire-erupts-in-San-15439395.php.

T. Tang. Train derails on arizona bridge that collapses, catches fire. *Associated Press*, 2020.

B. Evarts. *Fire Loss in the United States during 2018*. National Fire Protection Association, Quincy, MA, 2019.

Fire Protection Committee. *ASCE Manual No. 138: Structural Fire Engineering*. American Society of Civil Engineers, Reston, VA, 2018.

J. Stern-Gottfried, A. Law, G. Rein, M. Gillie, and J. Torero. *A Performance Based Methodology Using Travelling Fires for Structural Analysis*. Society of Fire Protection Engineers, Gaithersburg, MD, 2010.

National Institute of Standards and Technology. *Final Report on the Collapse of the World Trade Center Towers*, volume 13. U.S. Department of Commerce, Technology Administration, Washington, D.C., 2005.

B. Meacham, M. Engelhardt, and V. Kodur. Collection of data on fire and collapse. *Proceedings of NSF Engineering Research and Innovation Conference*, 2009. Honolulu, Hawaii.

B. Meacham, H. Park, M. Engelhardt, A. Kirk, V. Kodur, I. van Straalen, J. Maljaars, K. van Weeren, R. de Feijter, and K. Both. Fire and collapse: data collection and preliminary analyses. *Proceedings 8th International Conference on Performance-Based Codes and Fire Safety Design Methods*, 2010. Lund, Sweden.

N. Hironori. Investigation of Windsor Building Fire in Spain. *Report of Obayashi Corporation Technical Research Institute*, 2006. Kiyose, Japan.

C.R. Noble, A.P. Wemhoff, and L.D. McMichael. Thermal-structural analysis of the macarthur maze freeway collapse. *Proceedings Heat Transfer Summer Conference*, 48494:511–519, 2008.

M.T. Ahmadi, A.A. Aghakouchak, R. Mirghaderi, S. Tahouni, S. Garivani, A. Shahmariand, and S. Epackachi. Collapse of the 16-story Plasco Building in Tehran due to fire. *Fire Technology*, 56(2):769–799, 2020.

L. Bisby. Grenfell tower inquiry: Phase 1 Final Expert Report. University of Edinburgh, Edinburgh, 2018. https://www.grenfelltowerinquiry.org.uk/evidence/professor-luke-bisbys-expertreport-supplemental,last accessed 22/03/2019.

B. Lane. Grenfell tower–fire safety investigation. *Grenfell Tower Inquiry Hearing*, 2018. https://assets.grenfelltowerinquiry.org.uk/documents/Dr%20Barbara%20Lane%20report%20-%20section%201%20-%204.pdf.

J. Torero. Grenfell Tower: Phase 1 Report. *Report for the Grenfell Tower Inquiry*, 2018. https://www.grenfelltowerinquiry.org.uk/evidence/professor-jose-l-toreros-expert-report.

B. Henderson and C. Graham. Dubai skyscraper fire: torch tower residents wake to screams as flames engulf 79-storey building. *The Telegraph*, 3, 2017.

D.G. Lilley. Fire investigation: origin, cause and responsibility. *IECEC-97 Proceedings of the Thirty-Second Intersociety Energy Conversion Engineering Conference (Cat. No. 97CH6203),* Honolulu, HI, 1:631–635, 1997.

International Association of Fire Chiefs and International Association of Arson Investigators. *Fire Investigator: Principles and Practice to NFPA 921 and 1033*. 2014. Jones & Bartlett Publishers.

A.H. Buchanan and A.K. Abu. *Structural Design for Fire Safety*. John Wiley Sons, Ltd. Chichester, U.K., 2017.

P. Schulthess, M. Neuenschwander, K.M. Mosalam, and M. Knobloch. A computationally rigorous approach to hybrid fire testing. *Computers & Structures*, 238:106301, 2020. doi:https://doi.org/10.1016/j.compstruc.2020.106301.

C. Scawthorn. Water supply in regards to fire following earthquakes. *PEER Report No. 2011/08,* Pacific Earthquake Engineering Research Center, University of California, Berkeley, CA, 2011a.

C. Scawthorn. Fire following earthquake: Will water be there for firefighters? Pacific Earthquake Engineering Research Center, University of California, Berkeley, CA, 2011b. https://peer.berkeley.edu/sites/default/files/fire_following_earthquake-online-view-layout-sm.pdf.

C. Nolte. Pier 45 blaze adds another close call to mighty Jeremiah O'Brien's history. *San Francisco Chronicle*, 2020. https://www.sfchronicle.com/bayarea/nativeson/article/Mighty-Liberty-Ship-Jeremiah-O-Brien-survives-15304962.php.

M. Eslami, Rezaeian A., and V. Kodur. Behavior of steel column-trees under fire conditions. *J. Struct. Eng.*, 144(9):04018135, 2018.

V. Kodur, M. Yahyai, A. Rezaeian, M. Eslami, and A. Poormohamadi. Residual mechanical properties of high strength steel bolts subjected to heating-cooling cycle. *J. Construct. Steel Res.*, 131:122–131, 2017.

A.T. Anvari, M. Mahamid, M. McNallan, and M. Eslami. Effectiveness of damaged fire proofing in structural steel members subjected to fire. *J. Struc. Fire Eng.*, 2019. doi:DOI: 10.1108/JSFE-11-2017-0044.

R.H. White. *Charring Rates of Different Wood Species*. PhD thesis, Ph.D thesis, University of Wisconsin-Madison, Madison, WI.

American Wood Council. *National Design Specification for Wood Construction*. Leesburg, VA, 2012.

V. Babrauskas. Charring rate of wood as a tool for fire investigations. *Fire Safety J.*, 40(6):528–554, 2005.

D. Xie, G. Shan, and S. Lv. Oxidation behavior of carbon steel in simulated kerosene combustion atmosphere: a valuable tool for fire investigations. *Fire and Materials*, 42(2):156–163, 2018.

Z. Nodehi. Behaviour of structural glass at high temperatures. TU Delft, Masters Thesis, 2016. http://resolver.tudelft.nl/uuid:76278819-2c45-4110-8790-19ad87644678.

J.J. Lentini. Behavior of glass at elevated temperatures. *J. Forensic Sci.*, 37(5):1358–1362, 1992.

T.T. Lie. *SFPE Handbook of Fire Protection Engineering, Chapters 4-8*. 2nd edition, 1995.

C.R. Barnett. Bfd curve: A new empirical model for fire compartment temperatures. *Fire Safety J.*, 37(5):437–463, 2002.

European Committee for Standardization (CEN). Eurocode chapter 3: Design of steel structures-part 1-2: General rules-structural fire design. Brussels, Belgium, 2005.

B.R. Kirby, D.E. Wainman, T.L. Tomlinson, T.R. Kay, and B.N. Peacock. Natural fires in large scale compartments. *Int. J. Eng. Performance-Based Fire Codes*, 1(2):43–58, 1999.

D. Hibbitt, B. Karlsson, and P. Sorensen. *ABAQUS/Standard User's Manual, Version 6.19*. Dassault Systèmes Simulia Corp., Providence, RI, 2019.

Appendix A: Additional Photographs and Drawings

This appendix offers additional photographs and structural drawings of the damaged Pier 45.

Figure A.1: A typical undamaged column in Shed A.

Figure A.2: Damage as seen from the area between Shed A and Shed C.

Figure A.3: Failure of south-side perimeter columns as seen from the area between Shed A and Shed C.

Figure A.4: Anchor bolt pull out in west wall.

Figure A.5: Molten glass in west wall.

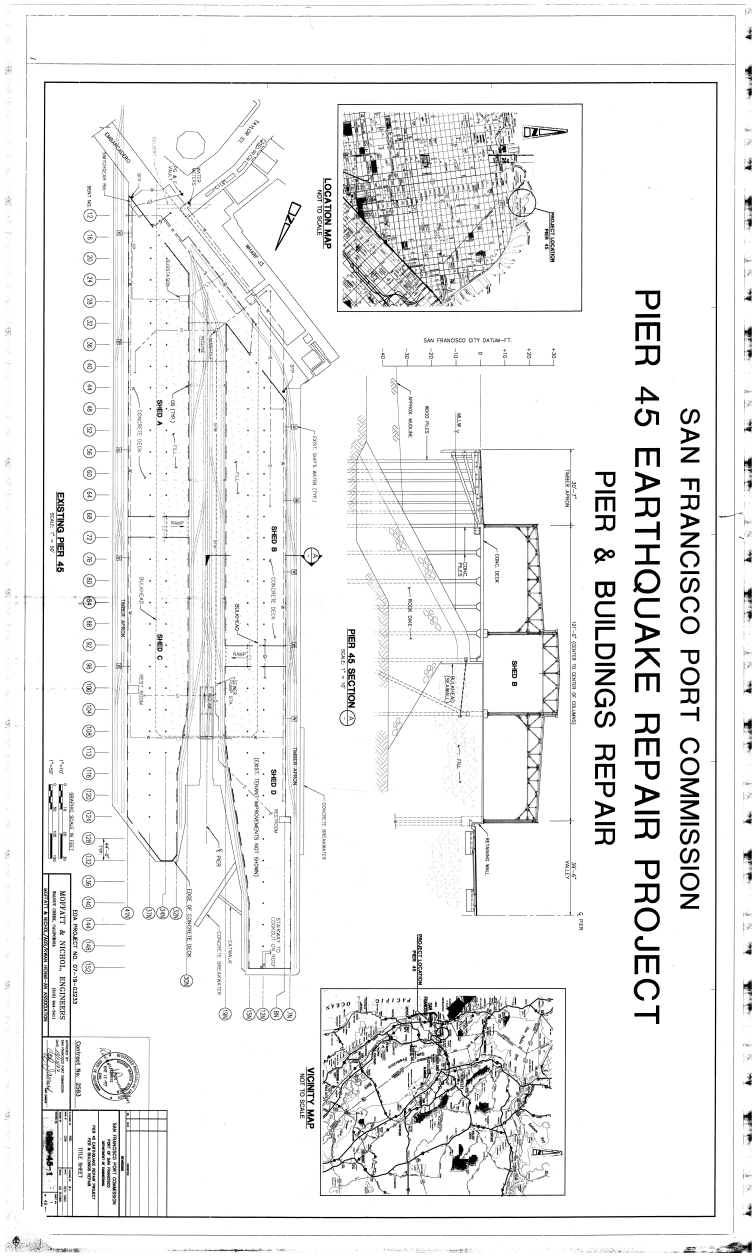

Figure A.6: Title sheet for Pier 45 earthquake repair project.

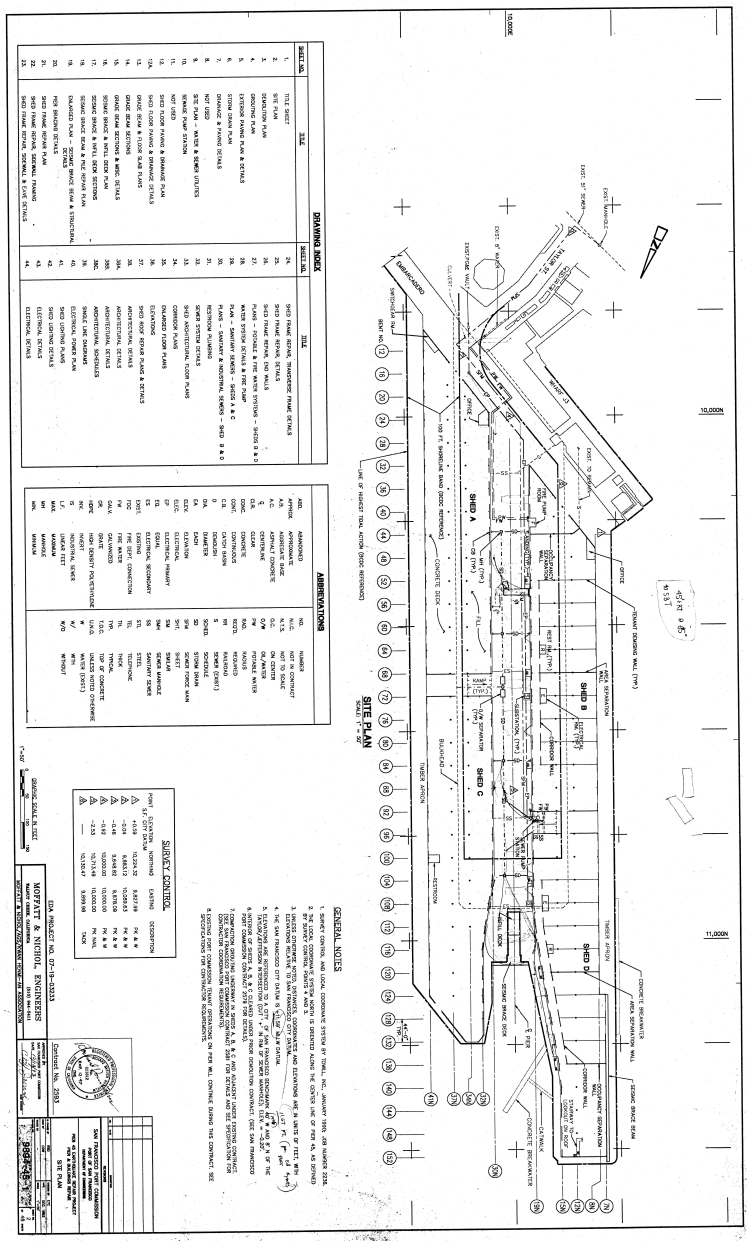

Figure A.7: Drawing index sheet for Pier 45 earthquake repair project.

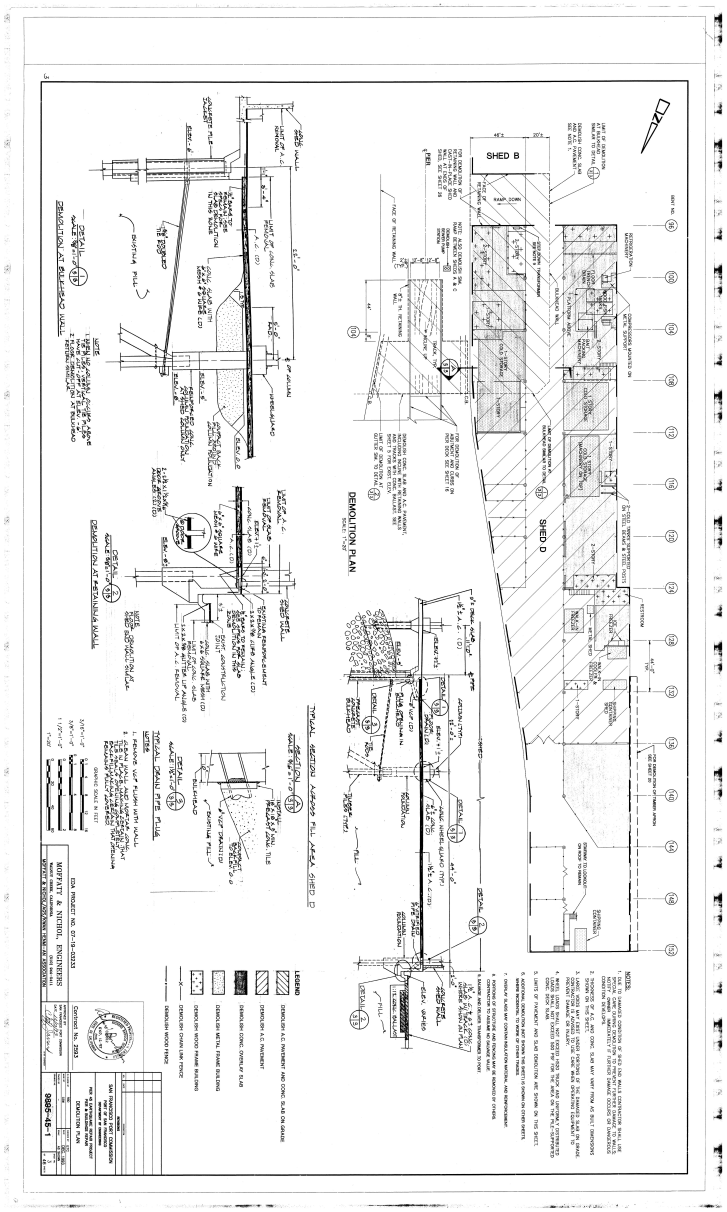

Figure A.8: Typical demolition plan (Shed D) for Pier 45 earthquake repair project.

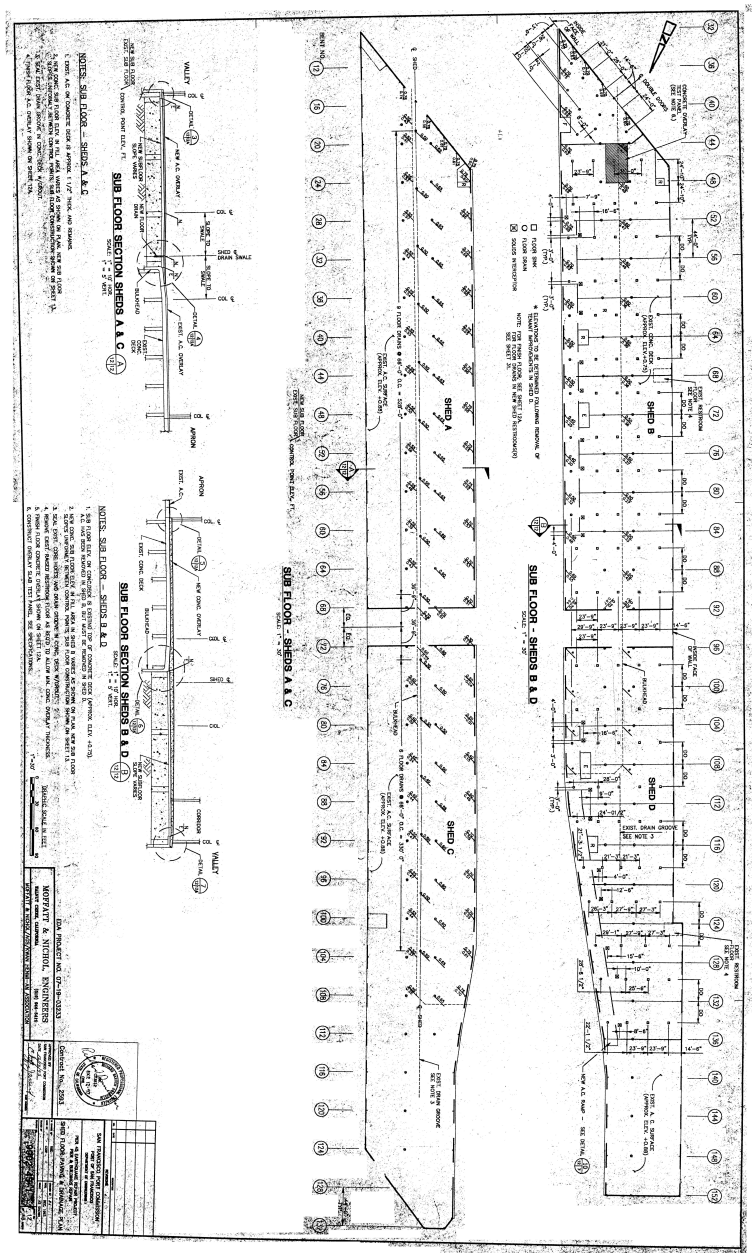

Figure A.9: Plans for sub-floor sections of all four sheds.

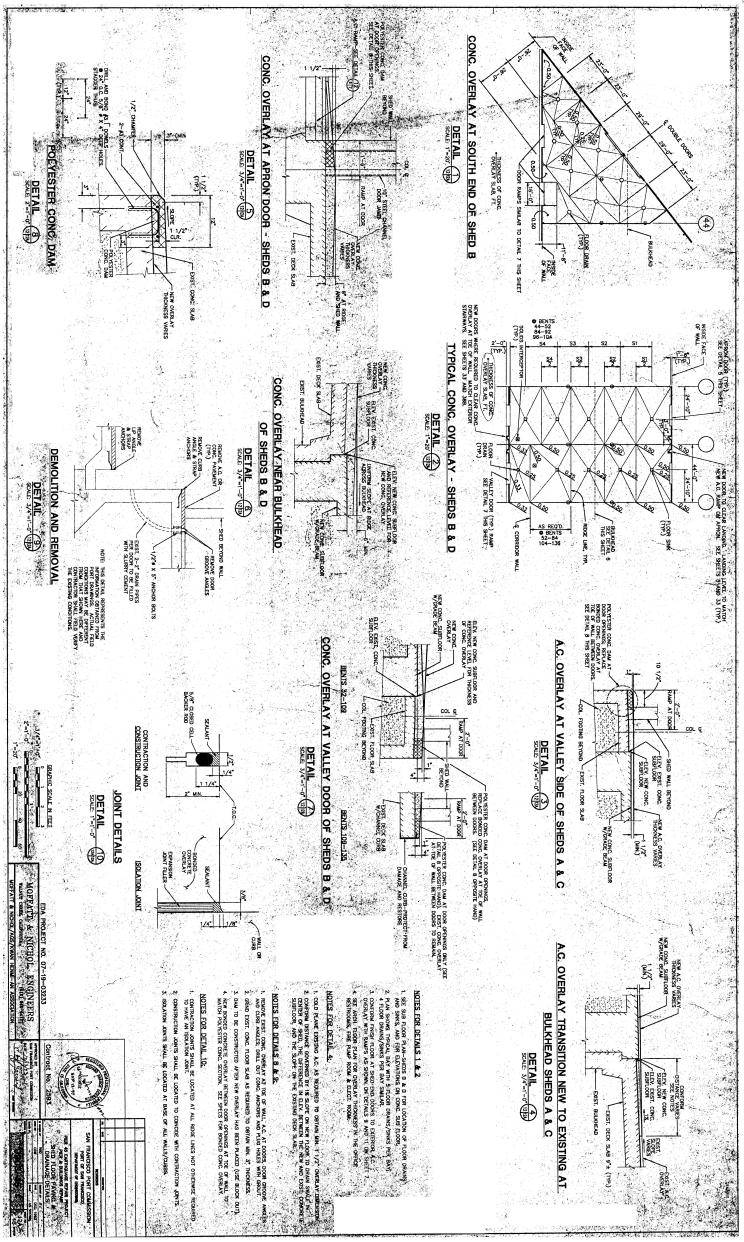

Figure A.10: Typical concrete overlay near doors and bulkheads for all four sheds.

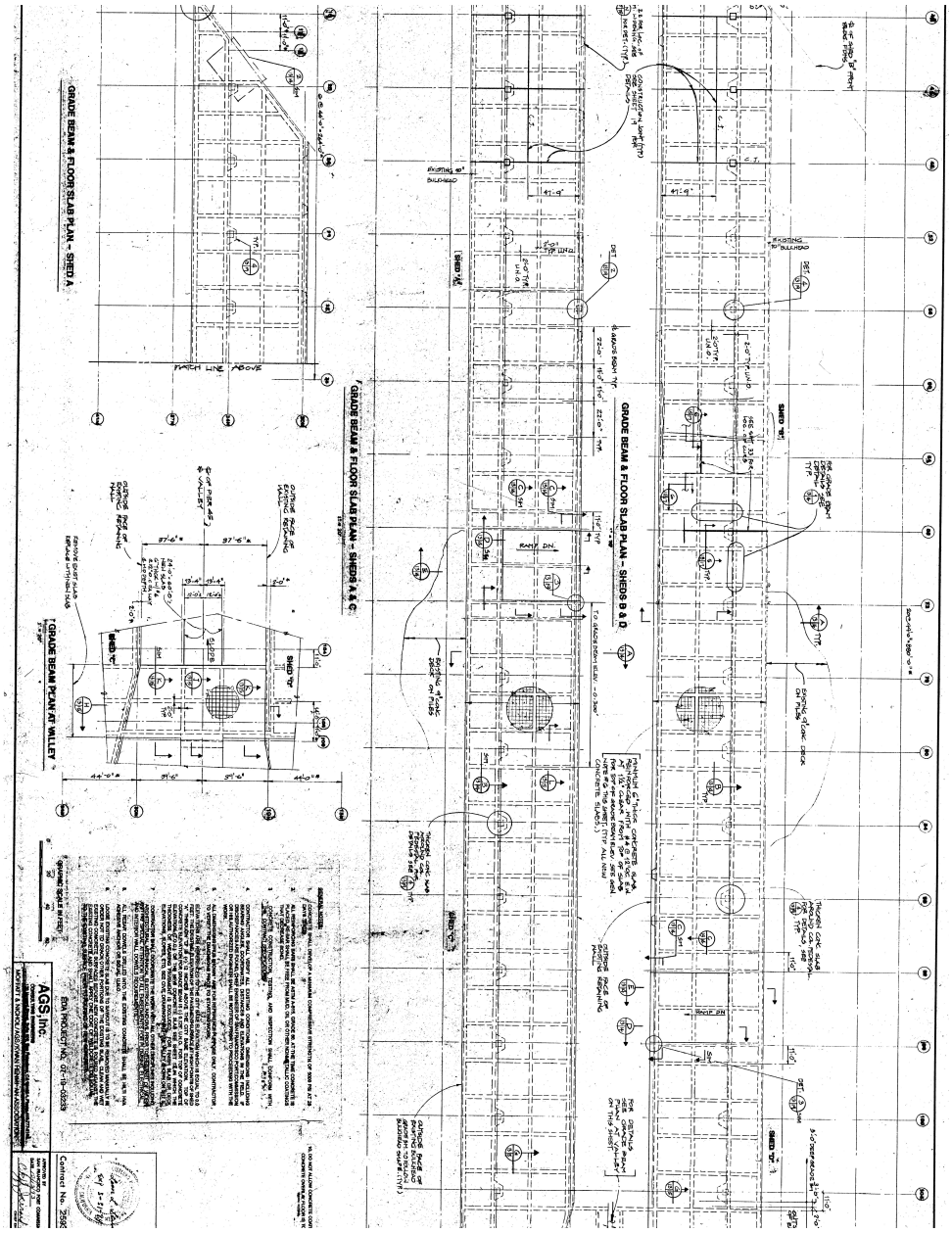

Figure A.11: Grade beam and floor slab plans of all four sheds.

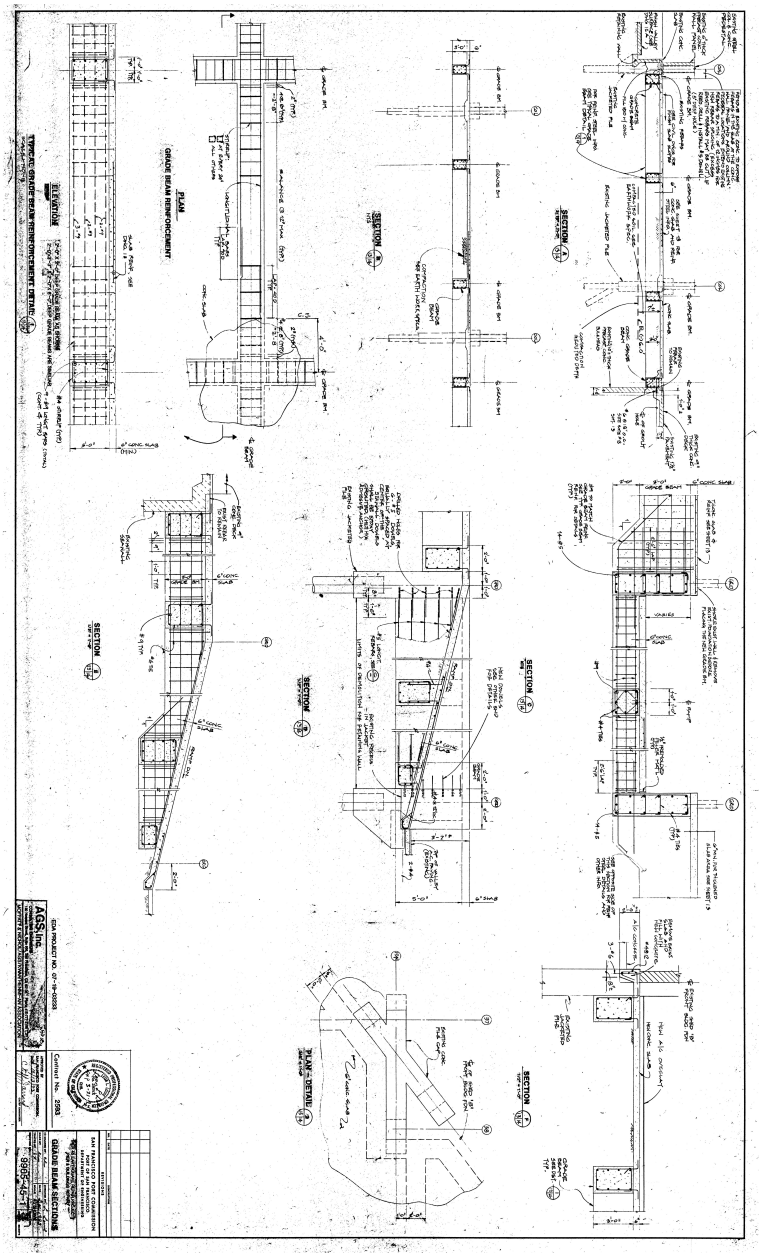

Figure A.12: Typical grade beam sections and reinforcing details.

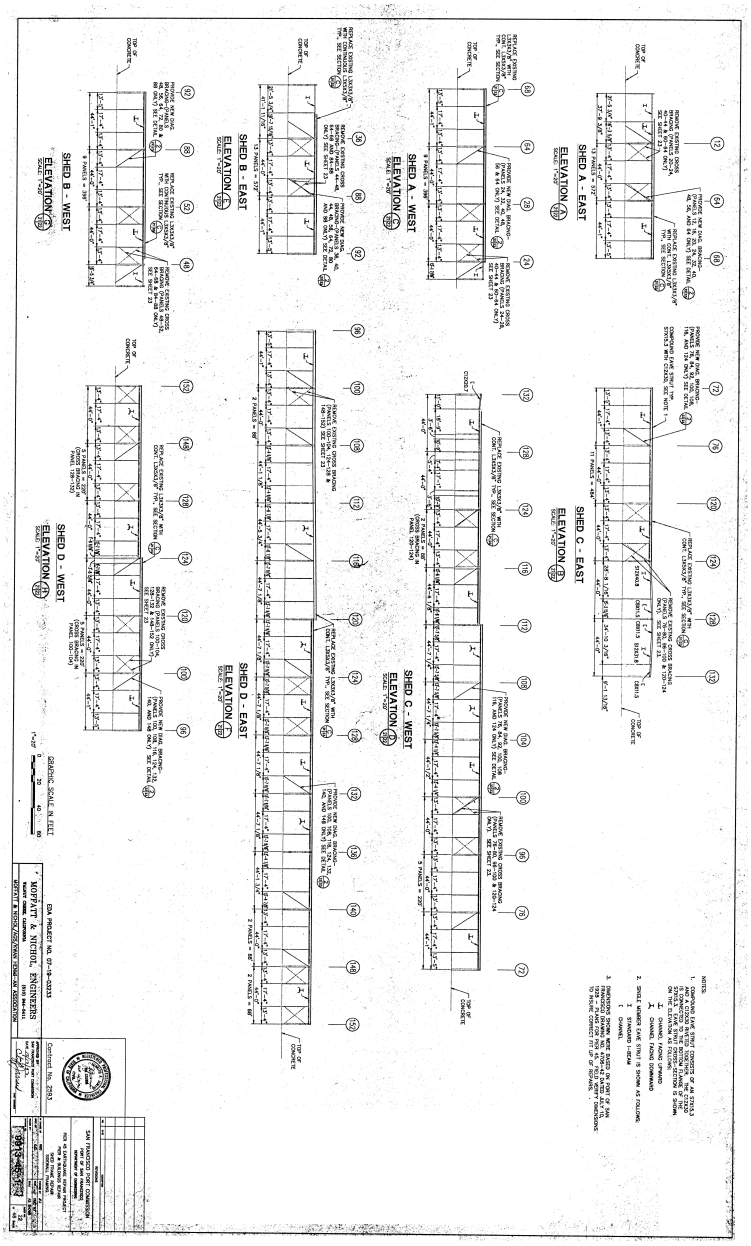

Figure A.13: Shed elevations based on drawing no. 4706-42 dated July 10, 1928.

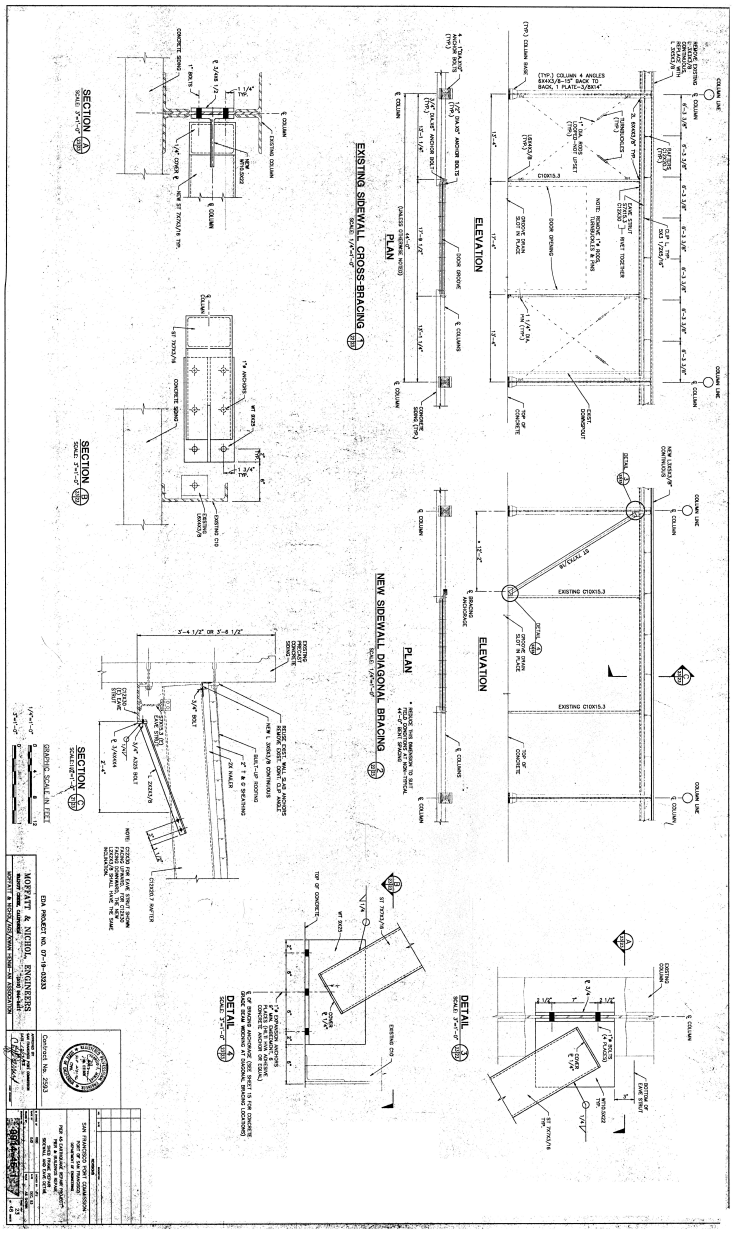

Figure A.14: Existing and new side wall bracing details.

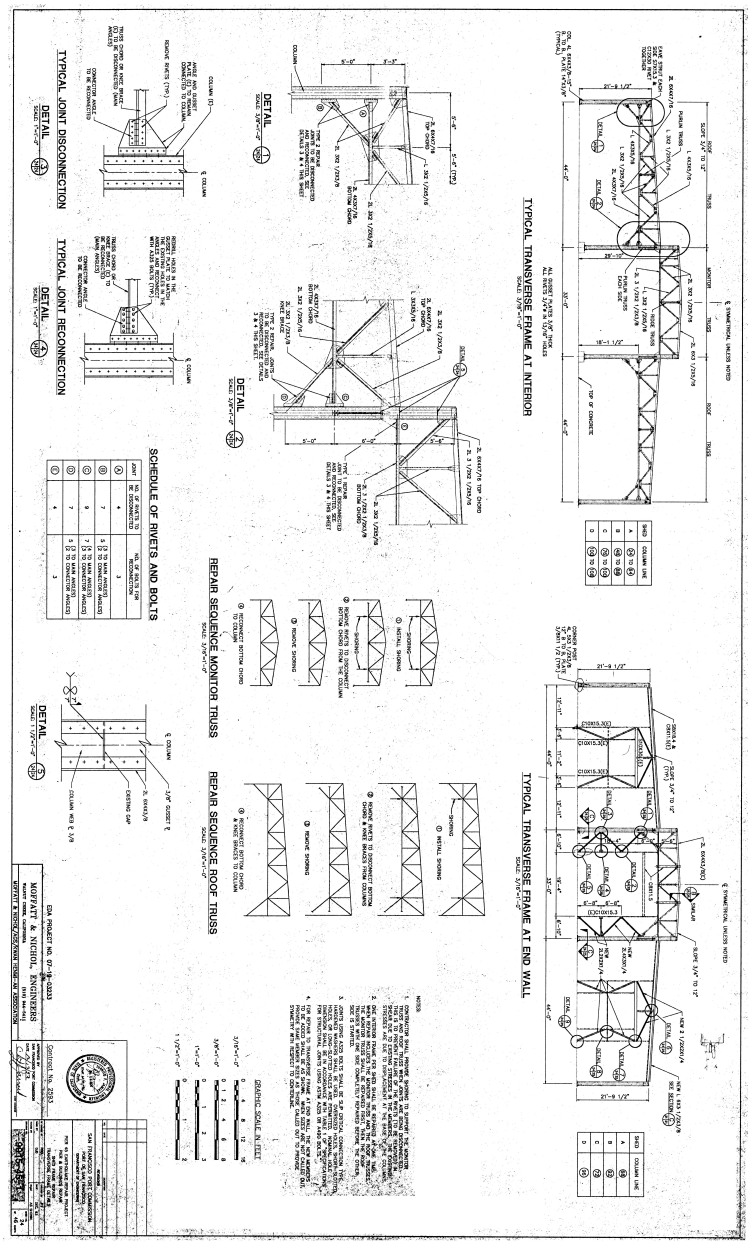

Figure A.15: Typical repair sequence and connection details of roof trusses.

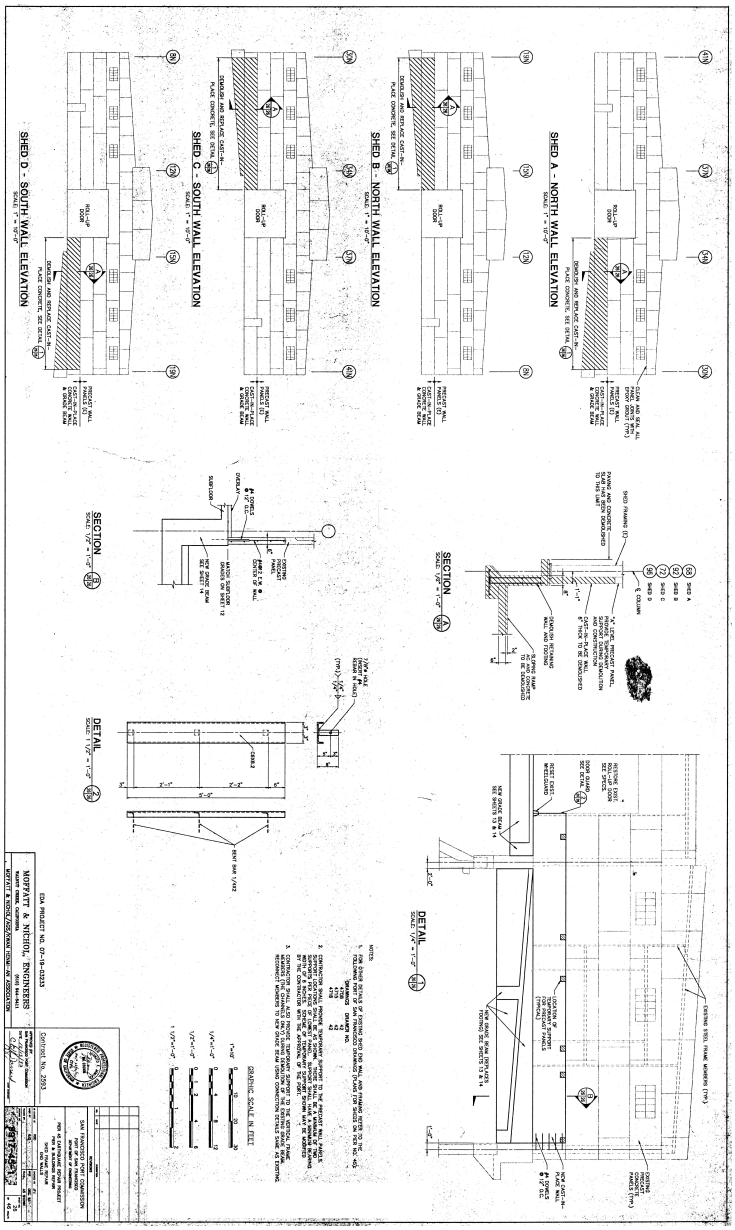

Figure A.16: Typical details of shed end walls.

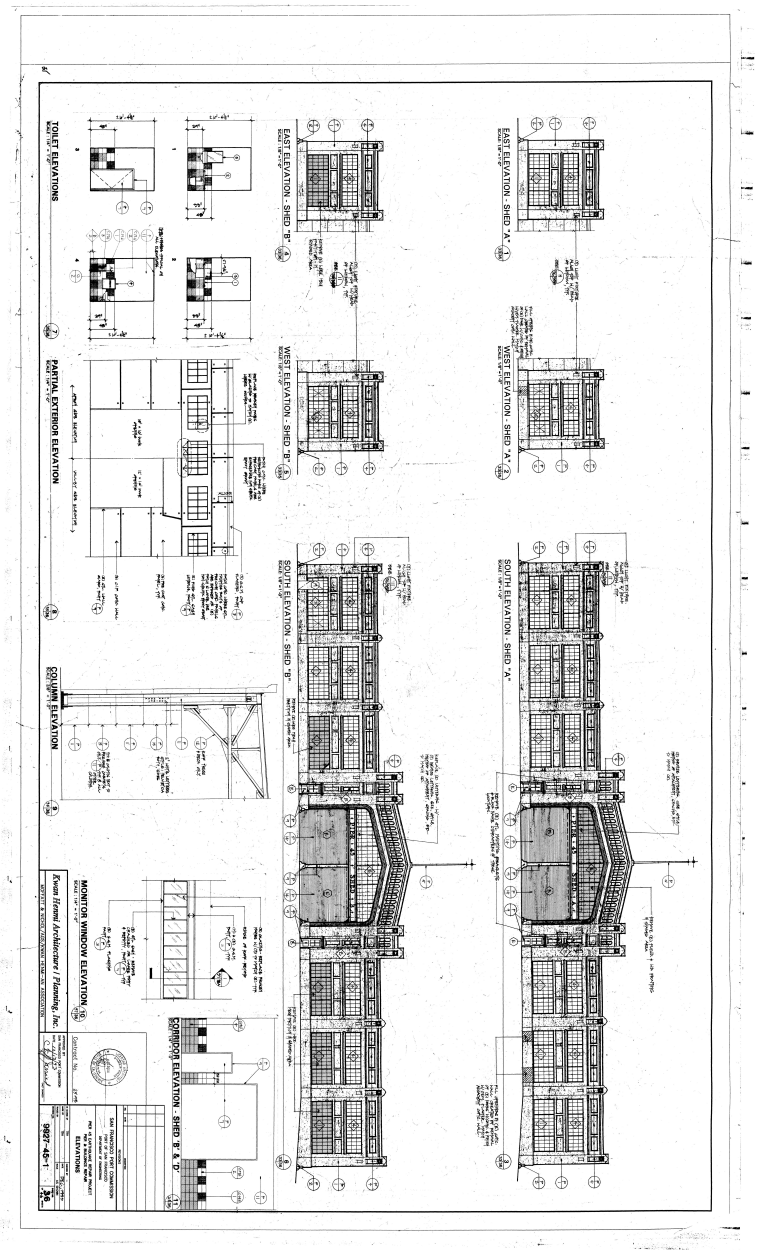

Figure A.17: Typical details of east and west elevation walls for Sheds A and B.

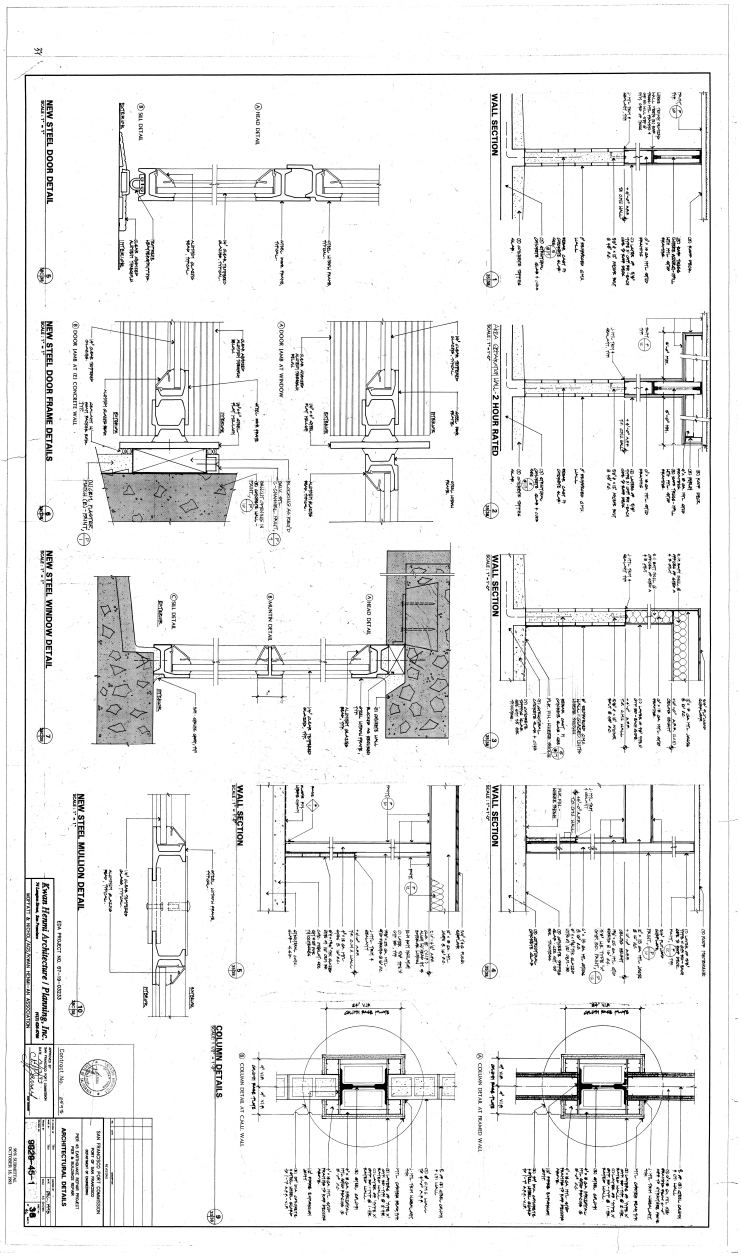

Figure A.18: Typical wall sections (including two-hour rated area separation wall), door frame, and window mullion details.

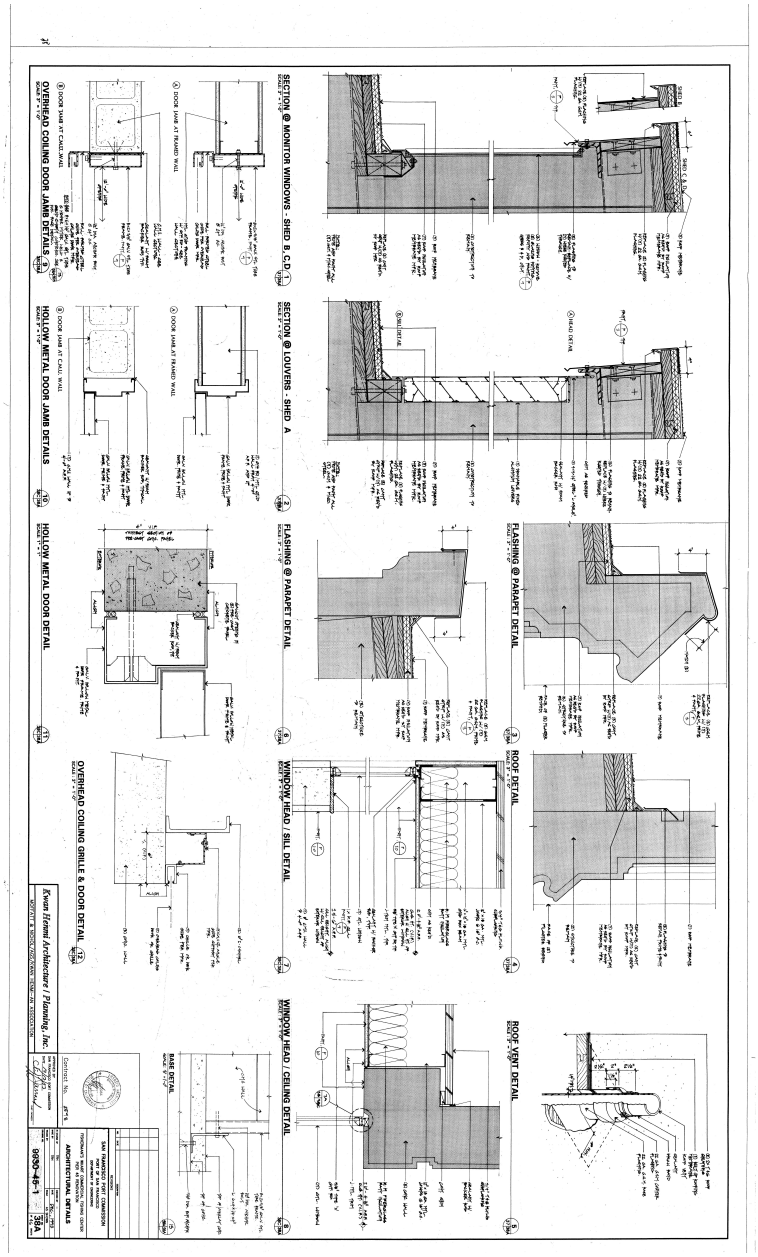

Figure A.19: Typical monitor window, louvers, parapet, ceiling, and coiling door details.

Figure A.20: Bending of column in the weak axis direction, with local buckling in flanges.

Figure A.21: Bending of column in the strong axis direction, with local buckling in the web.

Figure A.22: Remnant of an automobile.

Figure A.23: Forklifts with propane tanks (seen on the bottom right corner).

Figure A.24: An acknowledgment of presence of flammable materials.

Figure A.25: Corner of the building.

Figure A.26: Roof access stairs and damage on one side.

Figure A.27: Cracks in the concrete wall panel: diagonal at the edges and vertical at the center where the steel column provides support.

Figure A.28: Signs of heat-induced material flow in the compression flange of the steel beam.

Figure A.29: Molten glass on steel members, about 10 ft from the east edge, indicating an inward collapse of the glass panels at some locations on the eastern side.

Figure A.30: Buckling at the base of the HSS column section on the western side of the structure, indicating that the base plate pullout strength exceeded the section's flexural strength.

(a)

(b)

Figure A.31: Wall collapse and column buckling observations on the western side of the structure: (a) prevention of wall inward collapse because of a container; and (b) buckling of the column at mid-height can be seen.

Figure A.32: Intact gusset plate and connection between twisted steel members.

The Pacific Earthquake Engineering Research Center (PEER) is a multi-institutional research and education center with headquarters at the University of California, Berkeley. Investigators from over 20 universities, several consulting companies, and researchers at various state and federal government agencies contribute to research programs focused on performance-based earthquake engineering.

These research programs aim to identify and reduce the risks from major earthquakes to life safety and to the economy by including research in a wide variety of disciplines including structural and geotechnical engineering, geology/seismology, lifelines, transportation, architecture, economics, risk management, and public policy.

PEER is supported by federal, state, local, and regional agencies, together with industry partners.

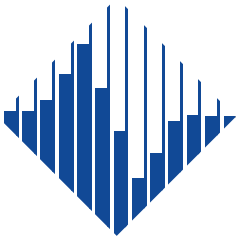

PEER Core Institutions

University of California, Berkeley (Lead Institution)
California Institute of Technology
Oregon State University
Stanford University
University of California, Davis
University of California, Irvine
University of California, Los Angeles
University of California, San Diego
University of Nevada, Reno
University of Southern California
University of Washington

PEER reports can be ordered at https://peer.berkeley.edu/peer-reports or by contacting

Pacific Earthquake Engineering Research Center
University of California, Berkeley
325 Davis Hall, Mail Code 1792
Berkeley, CA 94720-1792
Tel: 510-642-3437
Email: peer_center@berkeley.edu

ISSN 1547-0587X